ISCI, Volume *19*

Supplemental Information

Revealing the Critical Role of the HOMO Alignment on Maximizing Current Extraction and Suppressing Energy Loss in Organic Solar Cells

Jianyun Zhang, Wenrui Liu, Ming Zhang, Yanfeng Liu, Guanqing Zhou, Shengjie Xu, Fengling Zhang, Haiming Zhu, Feng Liu, and Xiaozhang Zhu

Supplemental Information

Revealing the Critical Role of the HOMO Alignment on Maximize Current Extraction and Suppress Energy Loss in Organic Solar Cells

Jianyun Zhang,[1,2,7] Wenrui Liu,[1,2,7] Ming Zhang,[4,7] Yanfeng Liu,[3] Guanqing Zhou,[4] Shengjie Xu,[1,*] Fengling Zhang,[3] Haiming Zhu,[5] Feng Liu,[4,*] and Xiaozhang Zhu[1,2,6,*]

[1]Beijing National Laboratory for Molecular Sciences, CAS Key Laboratory of Organic Solids, Institute of Chemistry, Chinese Academy of Sciences, Beijing 100190, China

[2]School of Chemical Sciences, University of Chinese Academy of Sciences, Beijing 100190, China

[3]Department of Physics, Chemistry and Biology (IFM), Linköping University, Linköping SE-581 83, Sweden

[4]School of Chemistry and Chemical Engineering, and Center for Advanced Electronic Materials and Devices, Shanghai Jiao Tong University, Shanghai 200240, China

[5]Department of Chemistry, Zhejiang University, Hangzhou 310027, China

[6]Lead Contact

[7]These authors contributed equally: Jianyun Zhang, Wenrui Liu, Ming Zhang

*Correspondence: xushengjie@iccas.ac.cn (S.X.), *fengliu82@sjtu.edu.cn (F.L.), *xzzhu@iccas.ac.cn (X.Z.)

1. Transport Method

Materials

The J71 was purchased from Solarmer Inc.; all materials were used in the condition they were received, without further purification. The molecular weight of polymer donor J71 is 18.573 kDa.

AFM

Atomic force microscopy (AFM) images of the thin films were obtained on a NanoscopeIIIa AFM (Digital Instruments) operating platform in tapping mode. The samples were prepared by spinning coated the active layers on the PEDOT:PSS layer.

TEM

Transmission electron microscopy (TEM) observation was performed on JEOL 2200 FS at 160 kV accelerating voltage. The samples for electron microscopy were prepared by dissolving the PEDOT:PSS layer using water and transferring the floating active layer to the TEM grids.

Scattering Characterization

The GIWAXS characterization of the thin films was performed at the Advanced Light Source (Lawrence Berkeley National Laboratory) on beamline 7.3.3. Samples were prepared under device conditions on the Si/PEDOT:PSS substrates. R-SoXS was performed at beamline 11.0.1.2 (ALS, LBNL). Samples were prepared under device conditions on the Si/PEDOT:PSS substrates, then placed in water and transferred to a silicon nitride window that obtained from CleanSiN.

PL Measurement

The pumping light source used to excite the samples was a green laser (532 nm), with a power of 10 mW. The PL spectra were recorded with an Andor spectrometer (Shamrock sr-303i-B), which was coupled with a Newton electron multiplying CCD (EMCCD) detector.

EL Measurement

An external current/voltage source was employed to provide an external electric field to the pristine and blended solar cells. The EL emissions were recorded with an Andor spectrometer.

FTPS-EQE Measurement

The FTPS-EQE was measured with a Vertex 70 from Bruker Optics, which was equipped with a quartz tungsten halogen lamp, quartz beam-splitter and external detector option. A low-noise current amplifier (SR570) was used to amplify the photocurrent produced under illumination of the solar cells, with light modulated by the Fourier transform infrared spectroscope (FTIR). The output voltage of the current amplifier was fed back into the external detector port of the FTIR to use the FTIR software to collect the photocurrent spectra.

EQE_{EL} Measurement.

The EQE_{EL} was recorded with an in-house-built system comprising a Hamamatsu silicon photodiode 1010B, Keithley 2400 source meter (for supplying voltages and recording injected currents), and Keithley 485 picoammeter (for measuring the emitted light intensity).

Transient Absorption Spectroscopy

For femtosecond transient absorption spectroscopy, the fundamental output from Yb:KGW laser (1030 nm, 220 fs Gaussian fit, 100 kHz, Light Conversion Ltd) was separated to two light beam. One was introduced to NOPA (ORPHEUS-N, Light Conversion Ltd) to produce a certain wavelength for pump beam (here we use 550 and 750 nm, 30 fs pulse duration), the other was focused onto a YAG plate to generate white light continuum as probe beam. The pump and probe overlapped on the sample at a small angle less than 10°. The transmitted probe light from sample was collected by a linear CCD array.

Device Development and Testing.

The devices were developed with a conventional structure of ITO/PEDOT:PSS/active layer/PDINO/Al. The ITO-coated glass substrates were cleaned with sequential ultrasonication in a soap-deionized water mixture, deionized water, acetone, and isopropanol. The washed substrates were further treated with oxygen plasma for 10 min to eliminate any remaining organic components. A thin layer (ca. 30 nm) of PEDOT:PSS (Clevios P VP 4083) was first spin-coated on the ITO substrates at 3,000 rpm and baked at 150 °C for 5 min under ambient conditions. The substrates were then transferred into a nitrogen-filled glove box. Subsequently, the active layers were spin coated from chloroform solution with the same optimal donor/acceptor (D/A) weight ratios of 1:1 for both J71: ZITI-S (or ZITI-C, ZITI-N, ZITI-C:ZITI-N) blends with a total concentration of 19 mg/mL. J71: ZITI-S blends was treated with thermal annealing at 100 °C, J71:ZITI-C, J71:ZITI-N and J71:ZITI-C:ZITI-N blends were treated with thermal annealing at 120 °C for 10 min. Then PDINO as the electron transporting layer was spin-coated on the active layer by 3000 rpm from alcohol solution. In the final stage, the substrates were pumped down in high vacuum, and aluminum (100 nm) was thermally evaporated onto the active

layer. Shadow masks were used to define the OSC active area (0.05 cm^2) of the devices. The current density–voltage (*J*–*V*) characteristics of the PV devices were measured under N_2 conditions using a Keithley 2400 source meter. An AAA grade solar simulator, with an air mass (AM) 1.5 global filter operated at 100 mW cm^{-2}, was used to simulate the AM 1.5G solar irradiation. The illumination intensity was corrected by using a standard monocrystalline silicon reference cell, with a protective KG5 filter calibrated by the National Renewable Energy Laboratory (NREL). The *J*-*V* curves were measured along the forward scan direction from –0.2 V to 1.5 V or the reverse scan direction from 1.5 V to –0.2 V, yielding identical results. The scan speed and dwell times were fixed at 0.015 V s^{-1} and 20 ms, respectively. The EQE was calculated using certified incident photon to current conversion efficiency (IPCE) equipment from Enlitech (Taiwan).

SCLC Mobility Measurements.

SCLCs were tested in electron-only devices configured with the ITO/ZnO/active layer/Al and hole-only devices configured with the ITO/PEDOT:PSS/active layer/MoO_3/Au. The mobilities were determined by fitting the dark-field current to the model of a single carrier SCLC current with field dependent mobility, which is described as

$$J = \frac{9\varepsilon_0\varepsilon_r\mu_0 V^2}{8L^3}$$

where *J* represents the current, μ_0 represents the zero-field mobility, ε_0 represents the permittivity of free space, ε_r represents the relative permittivity of the material, *V* represents the effective voltage, and *L* represents the thickness of the active layer. From the plot of $J^{1/2}$ vs *V*, the hole and electron mobilities can be deduced.

2. Synthetic Procedures

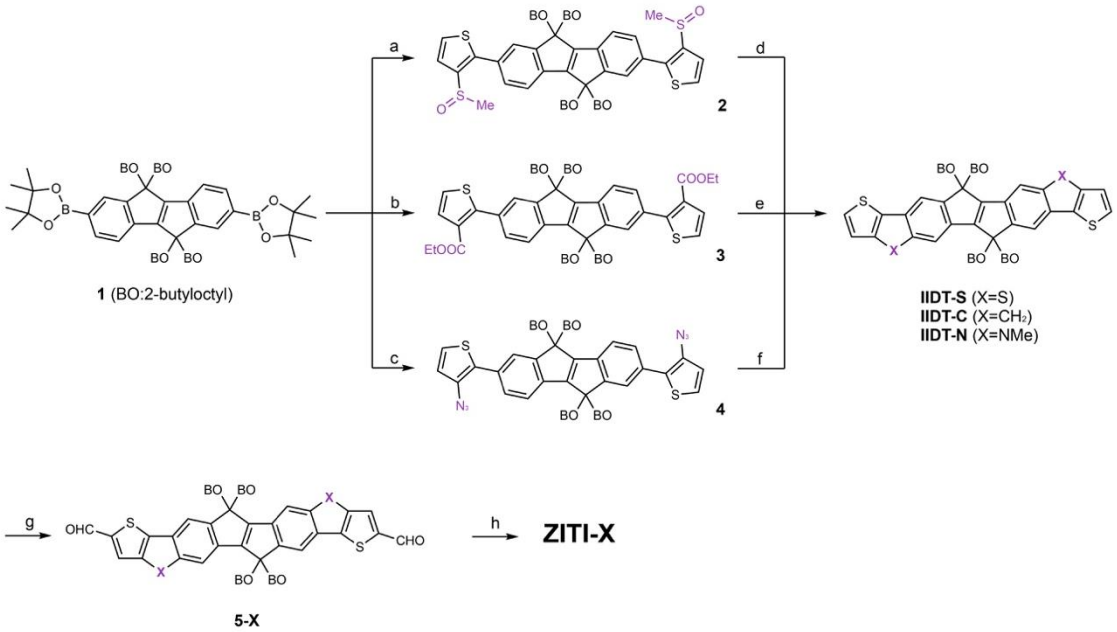

Supplementary Scheme 1 | Synthesis of ZITI-X NFAs. Reagents and conditions: **a**, 2-Bromo-3-(methylsulfinyl)thiophene, $Pd(PPh_3)_4$, aqueous Na_2CO_3, dioxane. **b**, Ethyl 2-bromothiophene-3-carboxylate, $Pd(PPh_3)_4$, aqueous Na_2CO_3, dioxane. **c**, (i) 2,3-Dibromothiophene, $Pd(PPh_3)_4$, THF. (ii) *n*-BuLi, Tos-N_3, THF; **d**, Eaton's reagent, pyridine. **e**, (i) KOH, ethanol; (ii) Oxalyl chloride, CH_2Cl_2, DMF. (iii) $AlCl_3$, CH_2Cl_2. **f**, (i) *o*-dichlorobenzene, 160 °C. (ii) NaH, CH_3I, DMF. **g**, $POCl_3$, DMF. **h**, INCN-2F, pyridine, $CHCl_3$.

Compound 2. Compound **1** (565 mg, 0.5 mmol) and 2-bromo-3-(methylsulfinyl)thiophene (338 mg, 1.5 mmol, 3 equiv.) were added to 19 mL of a 1:2 *v*/*v* mixture of aqueous Na_2CO_3 (2.0 M) and dioxanes under argon. The reaction mixture was purged with argon for 10 minutes and then $Pd(PPh_3)_4$ catalyst (58 mg, 0.05 mmol, 0.1 equiv.) was added. The reaction solution was stirred at 95 °C overnight under argon atmosphere and then was poured into ethyl acetate. The organic layer was washed with water and brine, and was dried over $MgSO_4$. The solvent was removed under reduced pressure. The resulting orange solid was purified on a silica-gel column chromatography to give 340 mg of compound **2** as a yellow solid (58%). ^{1}H NMR (300 MHz, $CDCl_3$): δ 7.63 (d, ^3J = 5.4 Hz, 2H), 7.62 (s, 2H), 7.43 (d, ^3J = 5.4 Hz, 2H), 7.40 (m, 4H), 2.75 (s, 6H), 2.04 (s, 8H), 1.20–0.60 (m, 92H); ^{13}C NMR (100 MHz, $CDCl_3$): δ 156.8, 145.4, 145.3, 145.2, 141.1, 139.6, 139.6, 132.0, 128.6, 127.8, 127.7, 127.5, 126.1, 126.0, 125.9, 125.6, 124.9, 124.8, 124.1, 120.3, 54.3, 44.9, 42.9, 42.2, 42.1, 35.0, 34.8, 34.7, 34.6, 34.5, 33.8, 33.7, 31.9, 31.8, 29.9, 29.8, 29.7, 28.1, 28.0, 27.9, 27.9, 27.8, 27.7, 25.9, 25.8, 25.7, 25.6, 23.1, 23.0, 22.7, 22.6, 14.2, 14.1, 14.0; HRMS (MALDI-TOF) calcd for $C_{74}H_{117}O_2S_4$ $[M+H]^+$: 1165.7931, found, 1165.7949.

Compound IDTT-S. Compound **2** (210 mg, 0.18mmol) was stirred with Eaton's reagent (8 mL) at room temperature in the dark for 3 days. The mixture was poured into ice-water, extracted with chloroform and the organic phase was dried with $MgSO_4$, the solvent was removed by reduced pressure and the crude product was dried in vacuum, which was followed to be redissolved in pyridine (10 mL) and then the mixture was refluxed overnight. After the mixture was cooled to room temperature, extracted with chloroform and diluted hydrochloride acid, the separated organic phase was dried over $MgSO_4$, and solvent was removed by reduced pressure. The crude was purified by column chromatography on silica gel column chromatography to afford a pale yellow solid **IDTT-S** (60 mg, 30 %). ^{1}H NMR (400 MHz, $CDCl_3$): δ 7.79 (s, 2H), 7.75 (s, 2H), 7.44 (d, ^3J = 5.2 Hz, 2H),

7.30 (d, ^3J = 4.8 Hz, 2H), 2.12 (m, 8H), 1.20–0.50 (m, 92H); ^{13}C NMR (100 MHz, $CDCl_3$): δ 156.0, 155.9, 155.8, 153.3, 153.2, 153.1, 141.6, 138.2, 138.1, 137.3, 137.2, 135.3, 129.2, 126.6, 120.4, 115.7, 115.6, 115.5, 114.5, 53.6, 53.4, 43.2, 43.0, 42.9, 42.8, 35.2, 35.0, 34.6, 34.5, 34.4, 34.3, 33.6, 31.9, 31.8, 29.9, 29.8, 29.7, 29.6, 28.5, 28.4, 27.7, 27.6, 26.2, 26.1, 25.28, 25.2, 25.1, 25.0, 23.1, 22.9, 22.8, 22.6, 14.1, 14.0, 13.9, 13.8; HRMS (MALDI-TOF) calcd for $C_{72}H_{108}S_4$ $[M]^+$: 1100.7328, found, 1100.7308.

Compound 4. Compound **1** (843 mg, 0.81 mmol) was dissolved in dry tetrahydrofuran, then slowly added a solution of 2,3-dibromothiophen (588 mg, 2.43 mmol, 3 equiv.) in tetrahydrofuran, $Pd(PPh_3)_4$ (94 mg, 0.081 mmol) was then added. The reaction solution was refluxed overnight at 95 °C. The organic layer was washed with water and brine, and was dried over $MgSO_4$. The solvent was removed under reduced pressure. The resulting orange solid was purified on a silica-gel column chromatography to give 530 mg yellow solid (54%). ^{1}H NMR (400 MHz, $CDCl_3$): δ 7.66 (s, 2H), 7.57 (d, ^3J = 7.6 Hz, 2H), 7.37 (d, ^3J = 7.6 Hz, 2H), 7.25 (m, 2H), 7.06 (t, ^3J = 5.6 Hz, 2H), 2.05 (s, 8H), 1.20–0.60 (m, 92H); ^{13}C NMR (100 MHz, $CDCl_3$): δ 156.5, 155.9, 140.5, 139.4, 131.8, 128.5, 127.3, 124.3, 123.9, 119.7, 106.9, 54.2, 42.9, 35.0, 34.9, 34.8, 34.6, 33.7, 31.9, 29.9, 29.7, 28.2, 27.8, 26.0, 25.6, 23.2, 23.0, 22.7, 14.1, 14.0; HRMS (MALDI-TOF) calcd for $C_{72}H_{110}Br_2S_2$ $[M]^+$: 1196.6410, found, 1196.6409. A solution of this yellow solid (500 mg, 0.42 mmol) in 20 mL of dry ether was added dropwise with stirring at -78 °C to n-butyllithium (0.63 mL, 1.6 M in n-hexane). The reaction mixture was stirred for 45 min at -78 °C, after which an ethereal solution of *p*-toluenesulfonyl azide (206 mg, 1.05 mmol) was added dropwise. After the addition was complete, the resulting mixture was stirred for 5 h at -78 °C. When the temperature had reached -10 °C, the resulting triazene salt was rapidly filtered off and washed with dry ether. The solid material was then suspended in 150 mL of ether and treated with a solution of 222 mg (0.82 mmol) of tetrasodium pyrophosphate in 10 mL of water. After the mixture was stirred overnight at 5 °C, the organic layer was separated, and the aqueous solution was extracted twice with ether, and was dried over $MgSO_4$. The solvent was removed under reduced pressure and used for the next step without further purification.

Compound IDTT-N. Compound **4** was stirred for 8 h at 160 °C in *o*-dichlorobenzene. The solvent was removed under reduced pressure. The resulting solid was purified on a silica-gel column chromatography to give 70 mg yellow solid (16%). ^{1}H NMR (400 MHz, $CDCl_3$): δ 8.08 (s, 2H), 7.65 (s, 2H), 7.33 (s, 2H), 7.27 (m, 2H), 7.05 (t, ^3J = 3.6 Hz, 2H), 2.05 (s, 8H), 1.25–0.50 (m, 92H); ^{13}C NMR (100 MHz, $CDCl_3$): δ 155.5, 148.0, 142.5, 140.8, 137.0, 125.1, 119.1, 118.8, 113.3, 111.3, 102.8, 53.0, 43.4, 35.2, 35.0, 34.2, 33.5, 32.0, 31.9, 31.8, 29.9, 29.8, 29.7, 28.4, 26.1, 23.1, 22.9, 22.6, 14.1, 14.0, 13.9; HRMS (MALDI-TOF) calcd for $C_{72}H_{110}N_2S_2$ $[M]^+$: 1066.8105, found, 1066.8104. A solution of this yellow solid (53 mg, 0.05 mmol) in 5 mL of dry DMF was added dropwise with stirring at 0 °C to NaH (10 mg, 0.25 mmol). The resulting mixture was stirred for 1 h at 25 °C, CH_3I (70 mg, 0.5 mmol) was then added into the mixture. The reaction solution was stirred overnight. The organic layer was washed with water and brine, and was dried over $MgSO_4$. The solvent was removed under reduced pressure. The resulting solid was purified on a silica-gel column chromatography to give 45 mg of **IDTT-N** as a yellow solid (80%).^{1}H NMR (400 MHz, $CDCl_3$): δ 7.66 (s, 2H), 7.29 (d, ^3J = 4.8 Hz, 2H), 7.24 (s, 2H), 7.06 (t, ^3J = 2.4 Hz, 2H), 3.91 (s, 6H), 2.15 (m, 8H), 1.15–0.50 (m, 92H); ^{13}C NMR (100 MHz, $CDCl_3$): δ 155.6, 147.4, 145.3, 141.6, 136.8, 124.8, 118.7, 116.5, 113.3, 110.0, 100.6, 53.1, 13.3, 35.2, 35.0, 34.4, 33.5, 32.1, 31.9, 31.8, 31.3, 30.0, 29.9, 29.7, 29.6, 28.5, 27.6, 26.2, 26.1, 25.1, 23.2, 23.1, 23.0, 22.6, 14.1, 14.0, 13.8; HRMS (MALDI-TOF) calcd for $C_{74}H_{114}N_2S_2$ $[M]^+$: 1094.8418, found, 1094.8418.

Compound 5-S. $POCl_3$ (22 μL, 0.23 mmol) was slowly added into 5 mL dry DMF under N2, after stirring at RT for 30 min. Compound **IDTT-S** (50 mg, 0.045 mmol) was added and the mixture was stirred at 70 °C overnight. The solvent was evaporated, and the residue was purified on a silica-gel column to give compound **5-S** (50 mg, 96%).^{1}H NMR (400 MHz, $CDCl_3$): δ 10.01 (s, 2H), 7.99 (s, 2H), 7.91 (s, 2H), 7.82 (s, 2H), 2.16 (s, 8H), 1.25–0.50 (m, 92H); ^{13}C NMR (100 MHz, $CDCl_3$): δ 181.9, 181.8, 156.5, 156.4, 156.3, 153.1, 153.0, 152.9, 143.5, 143.0, 141.7, 139.1, 136.6, 136.5, 136.4, 128.7, 127.6, 127.5, 115.8, 115.7, 115.6, 113.8, 52.8, 52.4, 42.0, 41.8, 41.7, 41.6, 34.2, 34.1,

33.9, 33.6, 33.5, 33.4, 33.3, 32.7, 30.9, 30.8, 30.7, 28.8, 28.6, 28.5, 27.5, 27.4, 26.6, 26.5, 26.4, 25.1, 25.0, 24.2, 24.1, 24.0, 23.9, 22.0, 21.8, 21.7, 21.6, 13.1, 13.0, 12.9, 12.8, 12.7; HRMS (MALDI-TOF) calcd for $C_{74}H_{109}O_2S_4$ $[M+H]^+$: 1157.7305, found, 1157.7202.

Compound 5-N. The synthesis method is similar to **5-S**. The starting material **IDTT-S** was replaced by **IDTT-N**. The final product was obtained as a dark-green solid (93% yield). ^{1}H NMR (400 MHz, $CDCl_3$): δ 9.94 (s, 2H), 7.76 (s, 2H), 7.71 (s, 2H), 7.29 (s, 2H), 3.94 (s, 6H), 2.17 (s, 8H), 1.30–0.50 (m, 92H); ^{13}C NMR (100 MHz, $CDCl_3$): δ 183.03, 182.9, 157.5, 157.4, 148.7, 148.6, 148.5, 144.7, 143.9, 142.2, 139.6, 139.5, 125.6, 118.3, 118.2, 118.1, 117.8, 114.8, 114.7, 101.1, 53.4, 43.2, 43.1, 35.3, 35.2, 35.0, 34.5, 34.4, 34.3, 33.7, 33.6, 32.0, 31.8, 31.7, 31.2, 29.9, 29.8, 29.7, 29.6, 28.6, 28.5, 27.5, 27.4, 26.3, 26.2, 25.1, 25.0, 24.9, 23.1, 22.9, 22.8, 22.6, 14.1, 14.0, 13.9, 13.8, 13.7; HRMS (MALDI-TOF) calcd for $C_{76}H_{114}N_2O_2S_2$ $[M]^+$: 1150.8316, found, 1150.8319.

Compound ZITI-S. INCN-2F (51 mg, 0.22 mmol) and compound **5-S** (50 mg, 0.043 mmol) were added to a solvent mixture of chloroform (10 mL) and pyridine (5 drops). The reaction was placed in an oil bath at 75 °C and was stirred for 18 hours. The mixture was directly purified on a silica-gel column chromatography using chloroform as eluent to give 45 mg of **ZITI-S** as black solid (66%). ^{1}H NMR (300 MHz, $CDCl_3$): δ 9.03 (s, 2H), 8.58 (m, 2H), 8.15 (s, 2H), 8.05 (s, 2H), 7.76 (s, 2H), 7.74 (t, ^3J = 7.5 Hz, 2H), 2.18 (s, 8H), 1.20–0.50 (m, 92H); HRMS (MALDI-TOF) calcd for $C_{100}H_{116}F_4N_4O_2S_2$ $[M]^+$: 1580.7575, found, 1580.7599.

Compound ZITI-C. The synthesis method is similar to **ZITI-S**. The starting material **5-S** was replaced by **5-CH$_2$**. The final product was obtained as a dark-green solid (61% yield). ^{1}H NMR (400 MHz, $CDCl_3$): δ 8.96 (s, 2H), 8.55 (m, 2H), 7.92 (s, 2H), 7.79 (s, 2H), 7.68 (t, ^3J = 7.6 Hz, 2H), 7.57 (s, 2H), 3.88 (s, 4H), 2.13 (s, 8H), 1.30–0.50 (m, 92H); ^{13}C NMR (150 MHz, $CDCl_3$): δ 186.2, 165.2, 159.2, 158.9, 157.2, 155.5, 155.4, 153.7, 153.6, 148.6, 142.8, 140.1, 138.8, 136.8, 134.8, 134.6, 120.2, 117.5, 117.1, 115.2, 115.0, 114.8, 114.7, 112.7, 112.5, 68.8, 54.4, 43.3, 43.1, 35.4, 35.1, 34.8, 34.1, 33.8, 32.2, 32.1, 32.0, 30.0, 29.9, 28.6, 27.9, 27.8, 26.3, 26.2, 25.5, 25.4, 23.3, 23.0, 22.9, 22.8, 14.2, 14.2, 14.0; HRMS (MALDI-TOF) calcd for $C_{100}H_{116}F_4N_4O_2S_2$ $[M]^+$: 1544.8470, found, 1544.8479.

Compound ZITI-N. The synthesis method is similar to **ZITI-S**. The starting material **5-S** was replaced by **5-NMe**. The final product was obtained as a dark-green solid (60% yield). ^{1}H NMR (400 MHz, $CDCl_3$): δ 8.99 (s, 2H), 8.54 (m, 2H), 7.92 (s, 2H), 7.82 (s, 2H), 7.69 (t, ^3J = 7.6 Hz, 2H), 7.28 (s, 2H), 3.95 (s, 6H), 2.19 (m, 8H), 1.20–0.50 (m, 92H); ^{13}C NMR (100 MHz, $CDCl_3$): δ 185.8, 159.6, 158.9, 155.7, 153.0, 149.4, 146.7, 146.3, 142.0, 138.8, 138.1, 136.8, 134.6, 124.0, 120.3, 118.8, 115.8, 115.0, 114.8, 114.7, 112.5, 112.3, 101.4, 68.0, 53.5, 43.1, 35.1, 34.9, 34.5, 33.8, 32.0, 31.8, 31.7, 31.4, 29.9, 29.8, 29.7, 29.6, 28.5, 27.4, 26.1, 25.0, 23.1, 22.9, 22.8, 22.6, 22.6, 14.1, 14.0, 13.9, 13.8; HRMS (MALDI-TOF) calcd for $C_{100}H_{118}F_4N_6O_2S_2$ $[M]^+$: 1574.8688, found, 1574.8691.

Abbreviations:

ITIC:
2,2’-[[6,6,12,12-tetrakis(4-hexylphenyl)-6,12-dihydrodithieno[2,3-*d*:2’,3’-*d*’]-*s*-indaceno[1,2-*b*:5,6-*b*’]dithiophene-2,8-diyl]bis[methylidyne(3-*oxo*-1*H*-indene-2,1(3*H*)-diylidene)]]bis[propanedinitrile]

BT-IC:
(4,4,10,10-tetrakis(4-hexylphenyl)-5,11-(2-ethylhexyloxy)-4,10-dihydrodithienyl[1,2-*b*:4,5-*b*’]benzodithiophene-2,7-diyl)bis[methylidyne(3-*oxo*-1*H*-indene-2,1(3*H*)-diylidene)]]bis[propanedinitrile]

BDT-IC:
2,2’-[[4,4,10,10-Tetrakis(4-hexylphenyl)-4,10-dihydrothieno[3’,2’:4,5]cyclopenta[1,2-*b*]thieno[2’’,3’’:3’,4’]cyclopenta[1’,2’:4,5]thieno[2,3-*f*][1]benzothiophene-2,8-diyl] bis[methylidyne(3-*oxo*-1*H*-indene-2,1(3*H*)-diylidene)]]bis[propanedinitrile]

NITI:
2,2’-[[6,6’-[5,5,10,10-tetrakis(2-hexyldecyl)-5,10-dihydroindeno[2,1-*a*]indene-2,7-diyl)bis(2-octylthieno[3,4-*b*]thiophene]-4,4’-diyl]bis[methylidyne(5,6-difluoro-3-*oxo*-1*H*-indene-2,1(3*H*)-diylidene)]]bis[propanedinitrile]

ZITI-S:
2,2’-[[6,6,13,13-tetrakis(2-butyloctyl)-6,13-dihydroindeno[1,2:2’,1’]indeno[5,6-*d:*5’,6’-*d*’]dithieno[3,2-*b:*3’,2’-*b*’]dithiophene-2,9-diyl]bis[methylidyne(5,6-difluoro-3-*oxo*-1*H*-indene-2,1(3*H*)-diylidene)]]bis[malononitrile]

ZITI-C:
2,2’-[[6,6,13,13-tetrakis(2-butyloctyl)-6,13-dihydro-*s*-indaceno[5,6:6’,5’]-*s*-indaceno[1,2-*b*:1’,2’-*b*’]dithiophene-2,9-diyl]bis[methylidyne(5,6-difluoro-3-*oxo*-1*H*-indene-2,1(3*H*)-diylidene)]]bis[malononitrile]

ZITI-N:
2,2’-[[6,6,13,13-tetrakis(2-butyloctyl)-4,11-dimethyl-4,6,11,13-tetrahydropentaleno[2,1-*f*:5,4-*f*’]dithieno[3,2-*b*:3’,2’-*b*’]diindole-2,9-diyl]bis[methylidyne(5,6-difluoro-3-*oxo*-1*H*-indene-2,1(3*H*)-diylidene)]]bis[malononitrile]

IIDT-S:
6,6,13,13-tetrakis(2-butyloctyl)-6,13-dihydro-*s*-indaceno[5,6:6’,5’]-*s*-indaceno[1,2-*b*:1’,2’-b’]dithiophene

IIDT-C:
6,6,13,13-tetrakis(2-butyloctyl)-6,13-dihydroindeno[1,2:2’,1’]indeno[5,6-*d:*5’,6’-*d*’]dithieno[3,2-*b:*3’,2’-*b*’]dithiophene

IIDT-N:
6,6,13,13-tetrakis(2-butyloctyl)-4,11-dimethyl-4,6,11,13-tetrahydropentaleno[2,1-*f:*5,4-*f*’]dithieno[3,2-*b*:3’,2’-*b*’]diindole

3. Supporting Figures and Tables

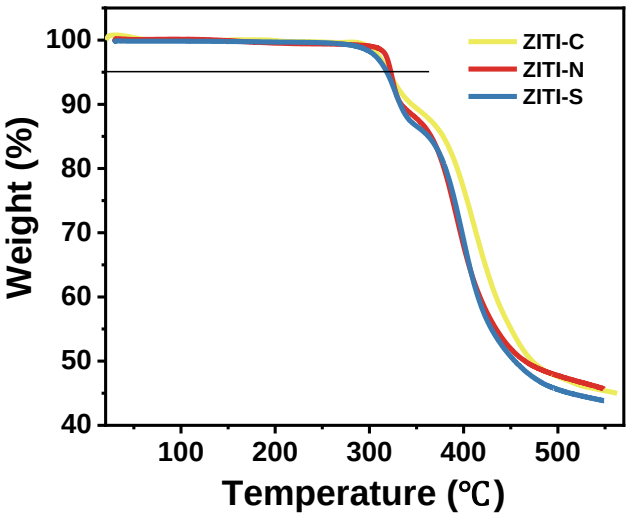

Figure S1. Thermal gravimetric analysis curves of ZITI-S, ZITI-C, and ZITI-N.

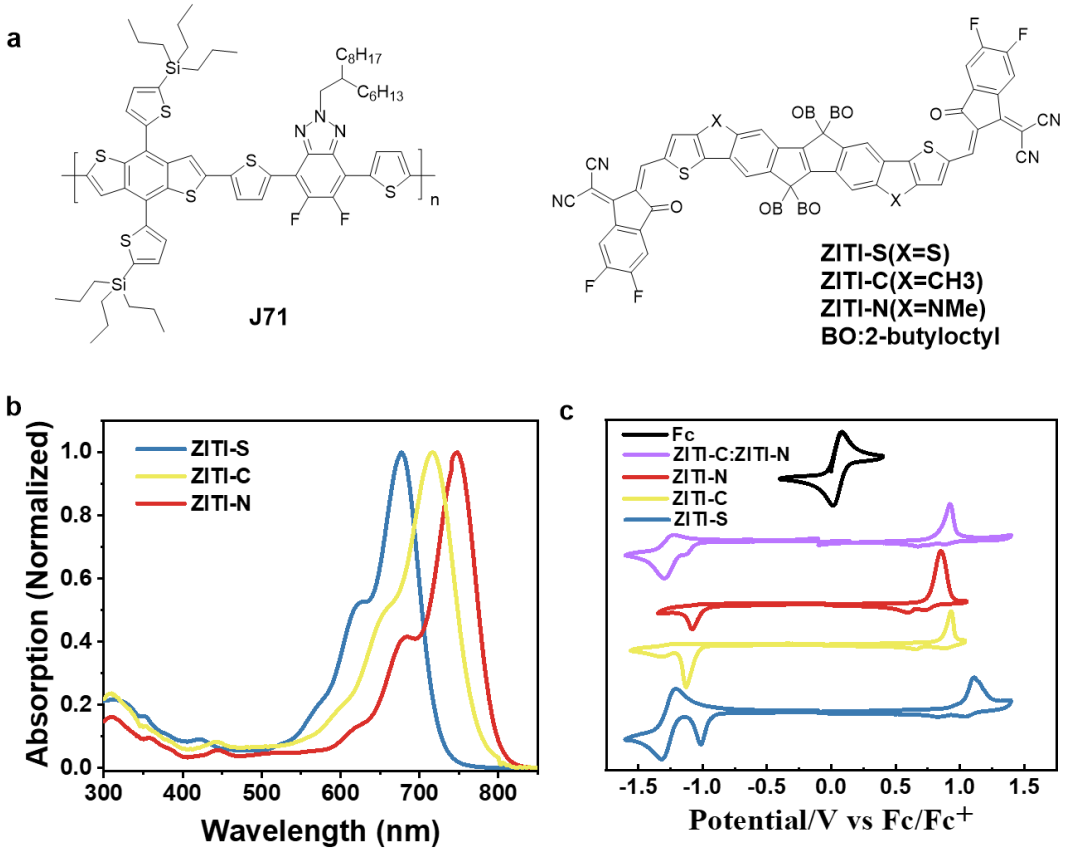

Figure S2. Photoelectric properties of ZITI-X. (a) The structure of the polymer and acceptors. (b) UV-vis-NIR absorption spectra of ZITI-S, ZITI-C, and ZITI-N in chloroform. (c) Cyclic voltammogram of ZITI-S, ZITI-C, ZITI-N, and ZITI-C:ZITI-N film in diluted CH_3CN solution with a scan rate of 100 mV s^{-1}.

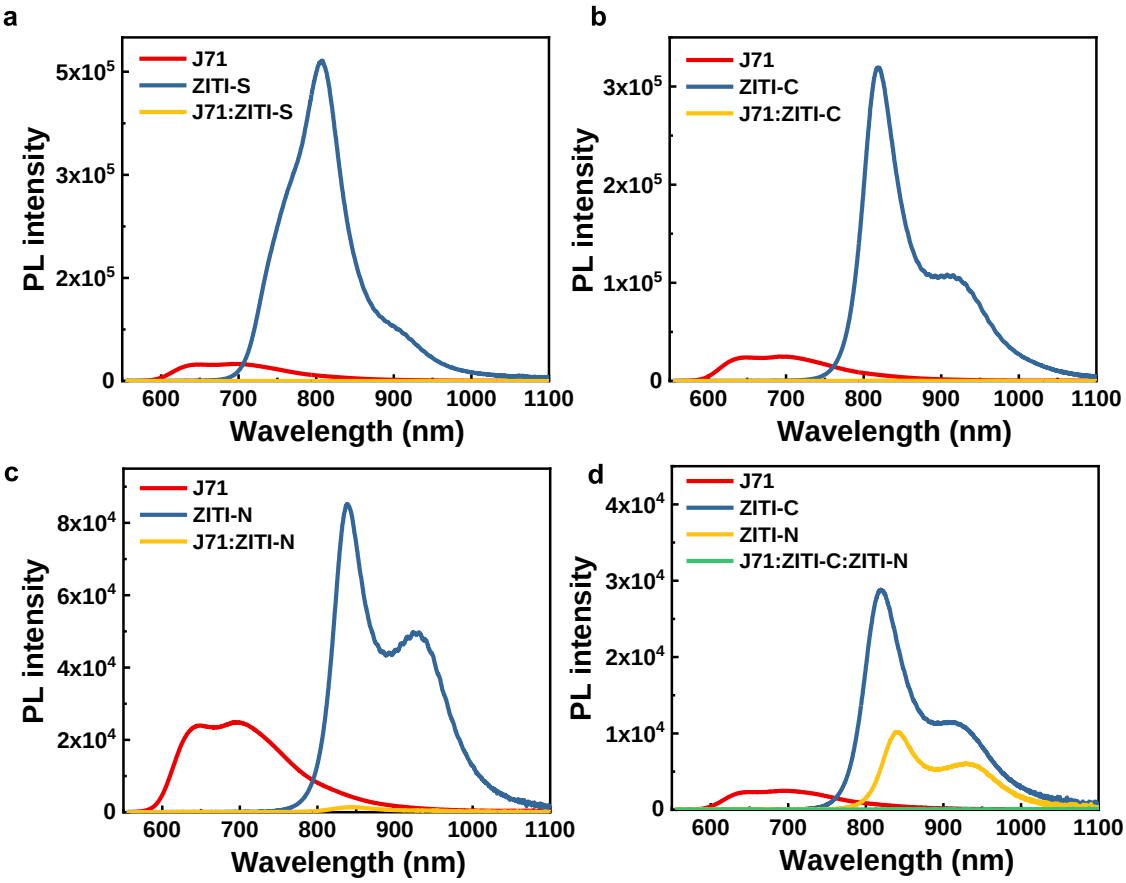

Figure S3. PL quenching. PL spectra of (a) the pristine donor J71, ZITI-S, and blended films, (b) the pristine donor J71, ZITI-C, and blended films, (c) the pristine donor J71, ZITI-N, and blended films, (d) the pristine donor J71, ZITI-C, ZITI-N, and blended films. For the PL measurements, the intensities are corrected by their absorptions at the excitation wavelength (532 nm).

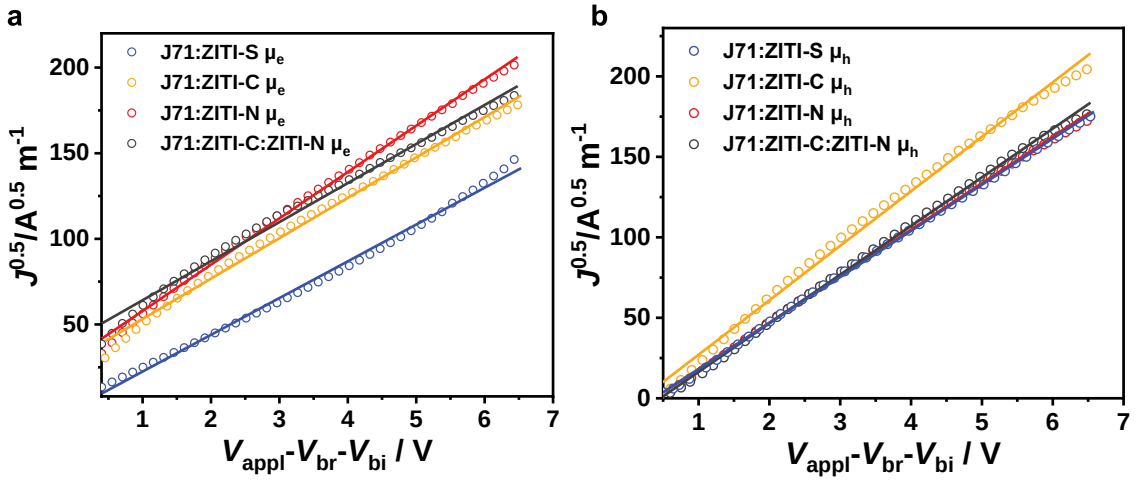

Figure S4. $J^{0.5}$ vs V plots of (a) electron-only diode and (b) hole-only diode in J71:ZITI-S, J71:ZITI-C, J71:ZITI-N, and J71:ZITI-C:ZITI-N blends.

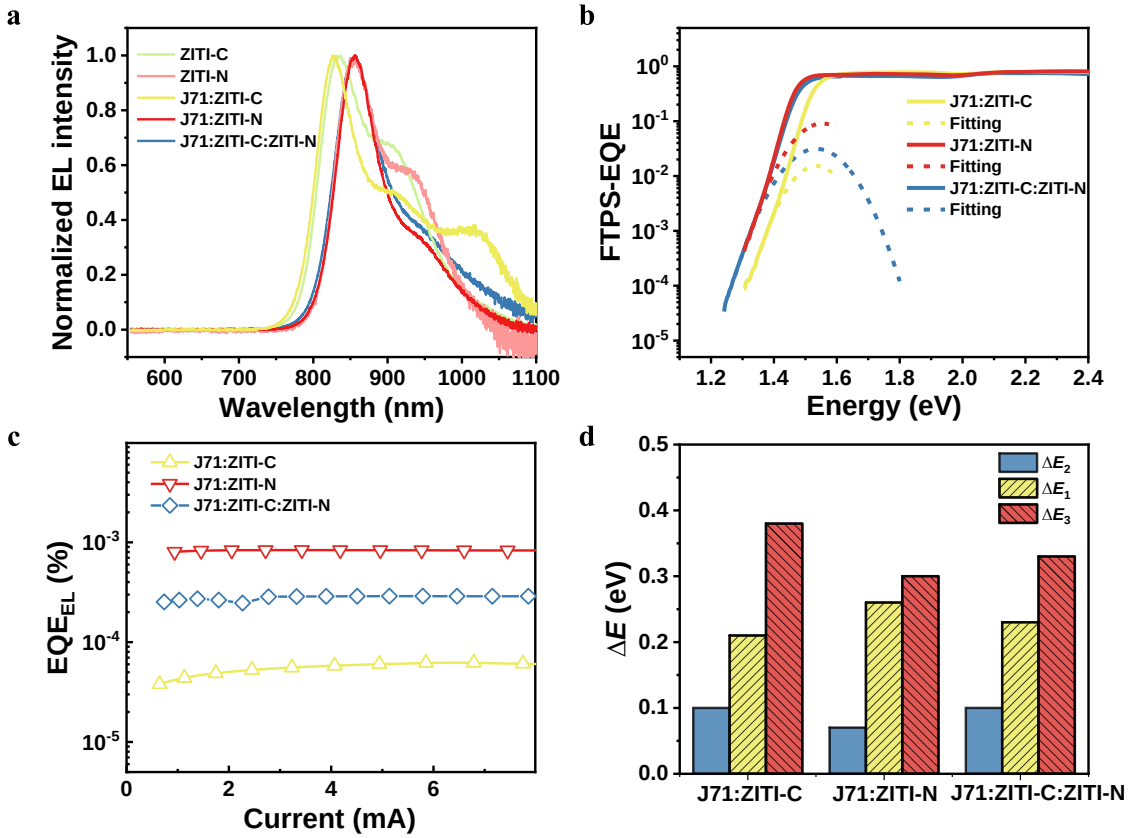

Figure S5. **Energy loss analysis.** (a) Electroluminescence spectra of devices based on the pristine NFA and blended films. (b) FTPS-EQE of the blended devices. (c) Normalized EQE$_{EL}$. (d) Energy loss: ΔE_1, ΔE_2 and ΔE_3 of J71:ZITI-C-, J71:ZITI-N-, and J71:ZITI-C:ZITI-N-based devices.

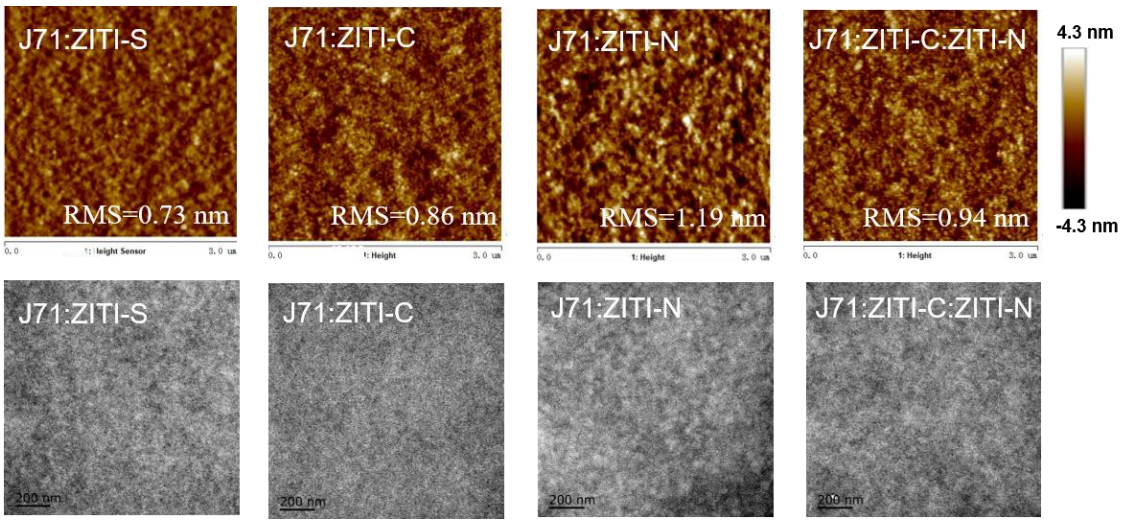

Figure S6. AFM height (3 × 3 μm) and TEM images of optimized blend films.

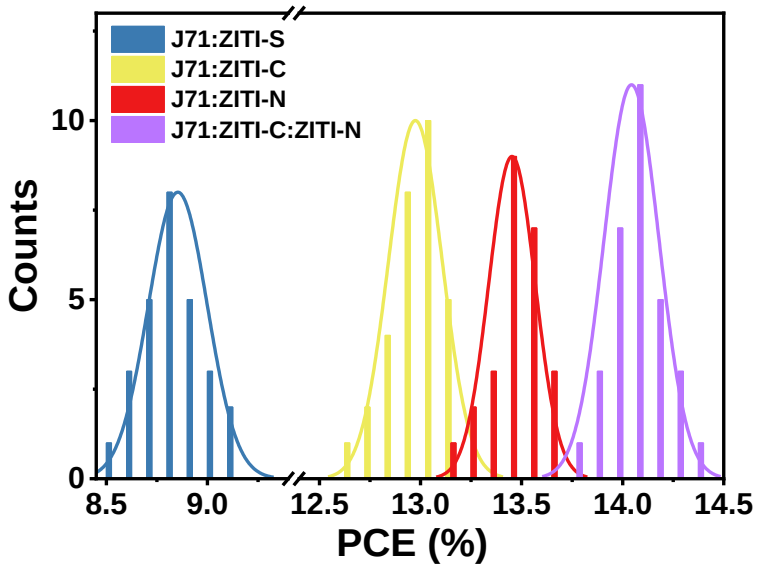

Figure S7. Histogram of the PCE measurements for 25 individual devices based on J71:ZITI-X blends.

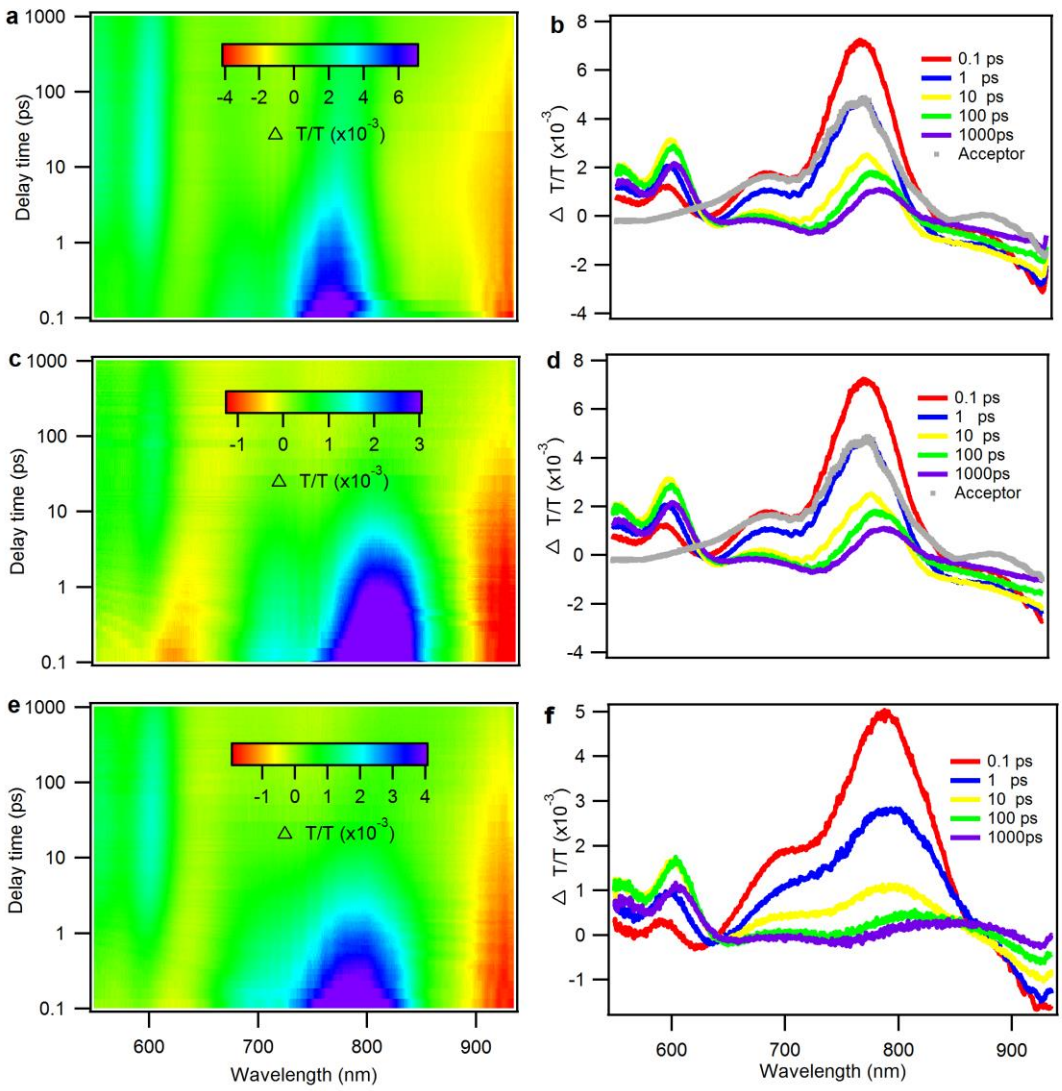

Figure S8. TAS investigation. Color plot of fs Transient absorption spectra of (a) J71:ZITI-C, (c) J71:ZITI-N and, (e) J71:ZITI-C:ZITI-N blend films at indicated delay times under 750 nm excitation with a fluence below 10 μJ/cm^2. Representative fs Transient absorption spectra of (b) J71:ZITI-C, (d) J71:ZITI-N, and (f) J71:ZITI-C:ZITI-N blend films at indicated delay time. Gray dots: TA spectrum of neat ZITI-C and ZITI-N film excited by 750 nm.

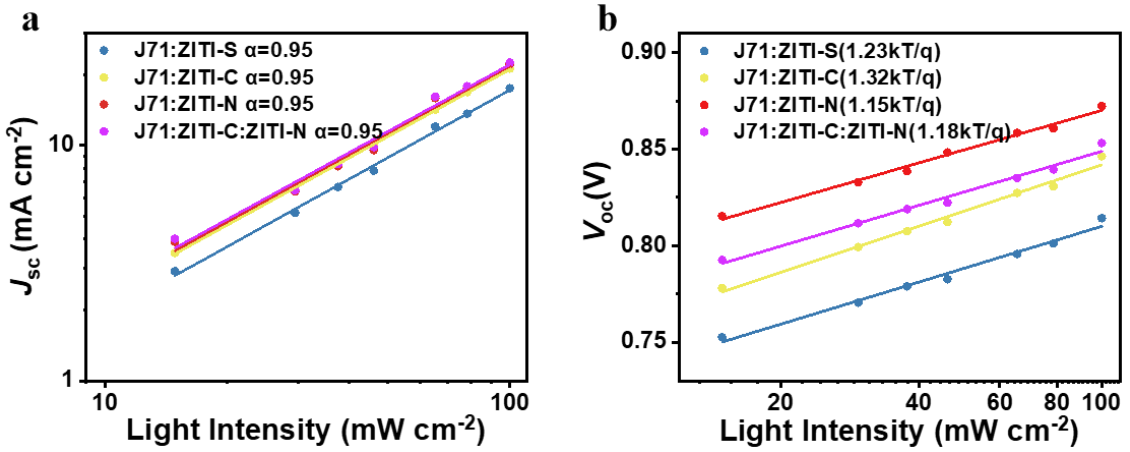

Figure S9. Charge recombination. (a) Measurement of J_{sc} versus light intensity. (b) V_{oc} versus light intensity for J71:ZITI-S-, J71:ZITI-C-, J71:ZITI-N-, and J71:ZITI-C:ZITI-N-based devices.

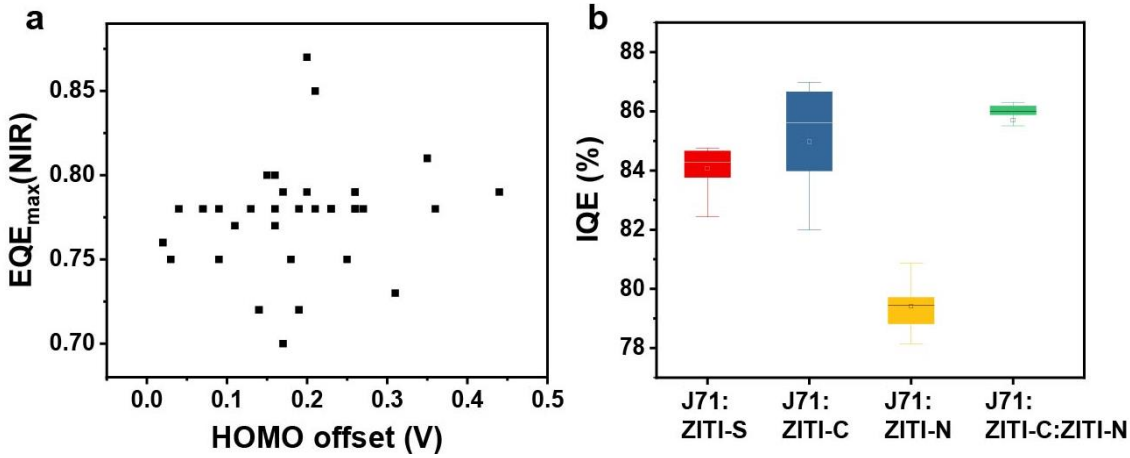

Figure S10. (a) EQE_{max} in NIR region against HOMO offset plots of the reported organic solar cells with efficiencies over 12%. (b) IQE response of J71:ZITI-X-based devices with different HOMO offsets.

Table S1. Photovoltaic performance of J71:(ZITI-S/ZITI-C/ZITI-N)-based solar cells with different D/A ratio with device structure of ITO/PEDOT:PSS/active layer/PDINO/Al. The average values with standard deviations were obtained from 10 devices.

	D:A	V_{oc} (V)	J_{sc} (mA cm^{-2})	**FF** (%)	**PCE** (%)
J71:ZITI-S	1:0.7	0.813±0.002	16.70±0.20	60.18±0.76	8.17±0.15 (8.37)
	1:1	0.812±0.004	17.18±0.38	63.51±0.87	8.86±0.18 (9.12)
	1:1.3	0.809±0.003	17.83±0.14	60.28±0.76	8.56±0.16 (8.81)
J71:ZITI-C	1:0.7	0.856±0.003	20.38±0.29	70.83±0.67	12.56±0.12 (12.70)
	1:1	0.851±0.006	21.28±0.26	72.03±0.79	13.02±0.13 (13.18)
	1:1.3	0.852±0.004	21.53±0.16	70.26±0.75	12.89±0.14 (13.13)
J71:ZITI-N	1:0.7	0.876±0.002	22.13±0.19	67.96±0.93	13.19±0.21 (13.42)
	1:1	0.873±0.005	21.73±0.33	70.96±0.88	13.47±0.12 (13.68)
	1:1.3	0.877±0.004	21.95±0.21	66.96±0.97	13.15±0.16 (13.30)

Table S2. Photovoltaic performance of J71:(ZITI-S/ZITI-C/ZITI-N)-based solar cells with different thicknesses. The average values with standard deviations were obtained from 10 devices.

	rpm	**Thickness** (nm)	V_{oc} (V)	J_{sc} (mA cm^{-2})	**FF** (%)	**PCE** (%)
J71:ZITI-S	4000	90	0.815±0.003	16.57±0.28	63.65±0.63	8.64±0.13 (8.82)
	3500	95	0.812±0.004	17.18±0.38	63.51±0.87	8.86±0.18 (9.12)
	3000	110	0.809±0.003	17.86±0.36	60.23±0.93	8.71±0.13 (8.90)
	2500	120	0.807±0.002	17.60±0.28	57.15±0.76	8.14±0.29 (8.38)
J71:ZITI-C	3500	95	0.849±0.005	20.38±0.19	73.13±0.86	12.71±0.15 (12.99)
	3000	110	0.851±0.006	21.28±0.26	72.03±0.79	13.02±0.13 (13.18)
	2500	120	0.850±0.004	21.08±0.17	70.98±0.83	12.99±0.16 (13.10)
	2000	135	0.847±0.003	21.37±0.25	69.88±0.73	12.94±0.12 (13.02)
J71:ZITI-N	3500	95	0.876±0.004	21.19±0.12	70.89±0.75	13.23±0.15 (13.46)
	3000	110	0.873±0.005	21.73±0.33	70.96±0.88	13.47±0.12 (13.68)
	2500	120	0.870±0.005	21.72±0.32	68.26±0.98	13.07±0.15 (13.21)

Table S3. Photovaltaic parameters of J71:(ZITI-S/ZITI-C/ZITI-N)-based devices before and after thermal annealing. The average values with standard deviations were obtained from 10 devices.

	TA	V_{oc} (V)	J_{sc} (mA cm^{-2})	FF (%)	PCE (%)
J71:ZITI-S	as-cast	0.835±0.003	16.37±0.21	54.27±0.86	7.42±0.20 (7.56)
	80℃/10 min	0.820±0.004	16.26±0.09	60.83±0.89	8.12±0.13 (8.23)
	100℃/10 min	0.812±0.004	17.18±0.38	63.51±0.87	8.86±0.18 (9.12)
	120℃/10 min	0.813±0.002	15.99±0.19	55.37±0.67	6.95±0.36 (7.30)
J71:ZITI-C	as-cast	0.899±0.005	19.58±0.24	66.53±0.74	11.64±0.12 (11.89)
	100℃/10 min	0.857±0.004	21.08±0.17	68.03±0.65	12.71±0.10 (12.87)
	120℃/10 min	0.851±0.006	21.28±0.26	72.03±0.79	13.02±0.13 (13.18)
	140℃/10 min	0.841±0.006	21.28±0.16	72.25±0.69	12.95±0.15 (13.09)
J71:ZITI-N	as-cast	0.913±0.004	20.73±0.29	61.61±0.74	11.68±0.15 (11.84)
	100℃/10min	0.883±0.002	21.93±0.21	65.07±0.86	12.66±0.22 (12.88)
	120℃/10min	0.873±0.005	21.73±0.33	70.96±0.88	13.47±0.12 (13.68)
	140℃/10 min	0.861±0.003	20.93±0.29	70.20±0.78	13.17±0.15 (13.28)

Table S4. Photovaltaic parameters of J71:ZITI-C:ZITI-N (D:A_1:A_2)-based devices. The average values with standard deviations were obtained from 20 devices.

D:A_1:A_2	V_{oc} (V)	J_{sc} (mA cm^{-2})	FF (%)	PCE (%)
1:1:0	0.851±0.006	21.28±0.26	72.03±0.79	13.02±0.13 (13.18)
1:0.7:0.3	0.851±0.003	22.62±0.32	70.32±0.88	13.54±0.17 (13.76)
1:0.6:0.4	0.858±0.006	22.73±0.24	70.29±1.07	13.56±0.20 (13.84)
1:0.5:0.5	0.857±0.004	23.01±0.24	71.72±0.98	14.05±0.21 (14.36)
1:0.4:0.6	0.861±0.004	22.43±0.23	72.17±0.67	13.92±0.16 (14.10)
1:0.3:0.7	0.865±0.006	22.39±0.33	70.76±0.78	13.70±0.16 (13.96)
1:0:1	0.873±0.005	21.73±0.36	70.96±0.88	13.47±0.12 (13.68)

Table S5. Charge transport properties of J71:ZITI-X blend films measured by SCLC method. The average values with standard deviations were obtained from 6 devices.

	μ_h ($cm^2\ V^{-1}\ s^{-1}$)	μ_e ($cm^2\ V^{-1}\ s^{-1}$)	μ_h:μ_e
J71:ZITI-S	2.75 (2.55±0.39)×10^{-4}	1.54 (1.46±0.17)×10^{-4}	1.78
J71:ZITI-C	3.83 (3.01±0.46)×10^{-4}	1.86 (1.83±0.35)×10^{-4}	2.05
J71:ZITI-N	2.69 (2.56±0.26)×10^{-4}	2.12 (2.01±0.27)×10^{-4}	1.27
J71:ZITI-C:ZITI-N	2.82 (2.69±0.43)×10^{-4}	2.24 (2.11±0.26)×10^{-4}	1.26

Table S6. Energy loss analysis.

	V_{oc} (V)	E_g^{opt} [a] (eV)	E_g^{inter} [b] (eV)	$q\Delta V_{oc}$ [c] ($q\Delta V_{oc}$) [d] (eV)	E_{CT} (eV)	ΔE_2 (eV)	ΔE_1 (eV)	EQE_{EL} (%)	ΔE_3 (eV)
J71:ZITI-S	0.81	1.61	1.66	0.80 (0.85)	1.36	0.30	0.20	2.54×10^{-5}	0.39
J71:ZITI-C	0.85	1.47	1.55	0.62 (0.70)	1.45	0.1	0.21	4.39×10^{-5}	0.38
J71:ZITI-N	0.88	1.41	1.51	0.53 (0.63)	1.44	0.07	0.26	8.16×10^{-4}	0.30
J71:ZITI-C:ZITI-N	0.86	1.41	1.51	0.55 (0.65)	1.41	0.1	0.23	2.64×10^{-4}	0.33

[a] E_g^{opt} is determined by thin-film absorption onset of an acceptor; [b] E_g^{inter} is determined at the intersection between absorption and emission of blend films; [c] $q\Delta V_{oc}=E_g^{opt}-qV_{oc}$; [d] $q\Delta V_{oc}=E_g^{inter}-qV_{oc}$.

Table S7. Photovoltaic performance of J71:ZITI-C:ZITI-N-based solar cells with different thicknesses. The average values with standard deviations were obtained from 10 devices.

	rpm	Thickness (nm)	V_{oc} (V)	J_{sc} (mA cm^{-2})	FF (%)	PCE (%)
J71:ZITI-C:ZITI-N =1:0.5:0.5	3500	95	0.854±0.005	22.88±0.17	72.07±0.67	13.85±0.24 (14.06)
	3000	110	0.857±0.004	23.01±0.24	71.72±0.98	14.05±0.21 (14.36)
	2500	120	0.853±0.004	22.95±0.16	69.94±0.68	13.79±0.21 (13.94)

Table S8. The EQE_{max} in NIR region against HOMO offset plots of the reported organic solar cells with efficiencies over 12%.

Active layer	PCE_{max} (%)	ΔE_{HOMO} (V)	NIR EQE_{max}	Reference
PBDB-T-2Cl:IT-4F	14.40	0.15	80%	1
PBDB-TF:ITPN	12.60	0.21	78%	2
PBT1-C:ITCPTC	12.80	0.16	77%	3
PBDB-T:F-Br	12.05	0.44	79%	4
PTQ10:IDIC	12.70	0.20	79%	5
PTB7-Th:IEICO-4F	12.80	0.20	87%	6
PBT1-C:TBTTT-2F	12.03	0.26	79%	7
PTQ10:IDTPC	12.20	0.26	78%	8
J71:ITCPTC	12.54	0.17	70%	9
J71:ZITI	13.24	0.11	77%	10
PBDTS-Se-TAZ:ITIC	12.31	0.19	78%	11
PTQ10:m-ITIC-4F	12.53	0.19	78%	12
PBDB-TF:IT-4F	13.70	0.13	78%	13
PDTB-EF-T:IT-4F	14.20	0.16	78%	14
PBDB-T-SF:NCBDT-4Cl	14.10	0.18	75%	15
PBDB-T:SN6IC-4F	13.20	0.19	72%	16
PBDB-T:IDT8CN-M	12.43	0.27	78%	17
PBDB-T:C8-ITIC	13.20	0.16	80%	18
PM7:IT-4F	13.10	0.17	79%	19
FTAZ: IOIC2	12.30	0.03	75%	20
PBDB-T:BDTThIT-M	12.12	0.04	78%	21
PBDTS-TDZ:ITIC	12.80	0.09	75%	22
PBDB-T-SF:IT-4F	13.10	0.26	79%	23
FTAZ:ITIC-Th1	12.10	0.36	78%	24
PBDB-T:NITI	12.74	0.35	81%	25
PBDB-TF:IDTN	12.20	0.31	73%	26
PBDB-T:IT-M	12.05	0.25	75%	27
PM6:Y6	15.70	0.09	78%	28
PTQ10:IE4F-S	12.20	0	68%	29
PBDB-T:IE4F-S	13.72	0.21	85%	29
J101:ZITI	14.43	0.23	78%	30
PDCBT:PDCBT-Cl	12.38	0.14	72%	31

PM7:IXIC-2Cl	13.72	0.07	78%	32
PBDB-T:BTTIC	13.18	0.26	78%	33
PCE10:3TT-OCIC	12.43	0.02	76%	34
PBDB-TF:BTP-4Cl	16.50	0.23	78%	35

Table S9. The photovoltaic parameters of J71:ZITI-N-based devices with different treatments.

Treatments	V_{oc} (V)	J_{sc} (mA cm^{-2})	FF (%)	PCE (%)
as-cast	0.913	20.73	61.61	11.84
120℃/10 min	0.876	21.78	72.00	13.68
0.5% DIO	0.951	12.33	42.84	5.03
0.5% 1-CN	0.970	11.08	50.28	5.41
CF 30s	0.919	20.82	63.38	12.13
THF 30s	0.905	20.85	63.14	11.92
CS2 30s	0.906	21.68	60.72	11.93

Table S10. The photovoltaic parameters of PBDB-TF:ZITI-C-, PBDB-TF:ZITI-N- and PBDB-TF:ZITI-C:ZITI-N-based devices.

Active layer	Treatments	V_{oc} (V)	J_{sc} (mA cm^{-2})	FF (%)	PCE (%)
PBDB-TF:ZITI-C	as-cast	0.934	20.00	65.82	12.31
	60℃/10 min	0.927	20.25	69.87	13.12
	100℃/10 min	0.903	20.47	67.25	12.43
	120℃/10 min	0.872	19.89	63.56	11.03
PBDB-TF:ZITI-N	as-cast	0.939	17.36	47.71	7.78
	60℃/10min	0.933	18.90	59.72	10.52
	80℃/10min	0.926	19.36	61.13	10.96
	120℃/10min	0.907	21.52	67.98	13.28
PBDB-TF:ZITI-C:ZITI-N=1:0.5:0.5	as-cast	0.942	19.98	63.17	11.89
	80℃/10 min	0.917	20.94	65.53	12.58
	100℃/10 min	0.905	21.40	67.88	13.15
	120℃/10 min	0.892	21.72	71.36	13.83

Table S 11. The photovoltaic parameters of polymer: ZITI-N-based devices.

Donor	treatment	V_{oc} (V)	J_{sc} (mA cm^{-2})	FF (%)	PCE (%)
PBDB-T-F	as-cast	0.939	17.36	47.71	7.78
	120℃/10 min	0.907	21.52	67.98	13.28

PBDB-T	as-cast	0.891	20.04	61.93	11.06
	120℃/10 min	0.839	22.20	70.74	13.17
PTB7-Th	as-cast	0.779	20.17	60.42	9.49
	120℃/10 min	0.764	21.17	69.92	11.31

Table S 12. The photovoltaic parameters of J71:ZITI-C:ZITI-N-based devices with different thickness.

Thickness (nm)	V_{oc} (V)	J_{sc} (mA cm^{-2})	FF (%)	PCE (%)
95	0.854	22.88	72.07	14.06
110	0.857	23.01	71.72	14.36
120	0.853	22.95	69.94	13.94
170	0.847	22.49	65.03	12.39
200	0.842	22.33	64.58	12.05

1. Zhang, S., Qin, Y., Zhu, J., and Hou, J. (2018). Over 14% efficiency in polymer solar cells enabled by a chlorinated polymer donor. Adv. Mater. *30*, 1800868.

2. Yu, R., Yao, H., Hong, L., Xu, Y., Gao, B., Zhu, J., Zu, Y. and Hou, J. (2018). Enhancing the photovoltaic performance of nonfullerene acceptors via conjugated rotatable end groups. Adv. Energy Mater. *8*, 1802131.

3. Xiong, W. *et al.* (2018). Controlling molecular weight to achieve high-efficient polymer solar cells with unprecedented fill factor of 79% based on non-fullerene small molecule acceptor. Sol. RRL *2*, 1800129.

4. Wang, Y. *et al.* (2018). A halogenation strategy for over 12% efficiency nonfullerene organic solar cells. Adv. Energy Mater. *8*, 1702870.

5. Sun, C., Pan, F., Bin, H., Zhang, J., Xue, L., Qiu, B., Wei, Z., Zhang, Z. G., and Li, Y. (2018). A low cost and high performance polymer donor material for polymer solar cells. Nat. Commun. ***9***, 743.

6. Song, X., Gasparini, N., Ye, L., Yao, H., Hou, J., Ade, H., and Baran, D. (2018). Controlling blend morphology for ultrahigh current density in nonfullerene acceptor-based organic solar cells. ACS Energy Lett. *3*, 669-676.

7. Song, J., Li, C., Ye, L., Koh, C., Cai, Y., Wei, D., Woo, H. Y., Sun, Y. (2018). Extension of indacenodithiophene backbone conjugation enables efficient asymmetric a–d–a type non-fullerene acceptors. J. Mater. Chem. A ***6***, 18847-18852.

8. Luo, Z., Sun, C., Chen, S., Zhang, Z., Wu, K., Qiu, B., Yang, C., Li, Y., and Yang, C. (2018). Side-chain impact on molecular orientation of organic semiconductor acceptors: High performance nonfullerene polymer solar cells with thick active layer over 400 nm. Adv. Energy Mater. *8*, 1800856.

9. Luo, Z. *et al.* (2018). Fine-tuning of molecular packing and energy level through methyl substitution enabling excellent small molecule acceptors for nonfullerene polymer solar cells with efficiency up to 12.54. Adv. Mater. *30*, 1706124.

10. Liu, W., Zhang, J., Zhou, Z., Zhang, D., Zhang, Y., Xu, S., and Zhu, X. (2018). Design of a new fused-ring electron acceptor with excellent compatibility to wide-bandgap polymer donors for high-performance organic photovoltaics. Adv. Mater. *30*, 1800403.

11. Li, Z., Xu, X., Zhang, G., Yu, T., Li, Y., and Peng, Q. (2018). Highly efficient non-fullerene polymer solar cells enabled by wide bandgap copolymers with conjugated selenyl side chains. Sol. RRL *2*, 1800186.

12. Li, X. J. *et al.* (2018). Improvement of photovoltaic performance of polymer solar cells by rational molecular optimization of organic molecule acceptors. Adv. Energy Mater. *8*, 1800815.

13. Li, W., Ye, L., Li, S., Yao, H., Ade, H., Hou, J. A high-efficiency organic solar cell enabled by the strong intramolecular electron push-pull effect of the nonfullerene acceptor. *Adv. Mater.* **30**, 1707170 (2018).

14. Li, S., Ye, L., Zhao, W., Yan, H., Yang, B., Liu, D., Li, W., Ade, H., and Hou, J. (2018). A wide band gap polymer with a deep highest occupied molecular orbital level enables 14.2% efficiency in polymer solar cells. J. Am. Chem. Soc. *140*, 7159-7167.

15. Kan, B., Feng, H., Yao, H., Chang, M., Wan, X., Li, C. X., Hou, J., and Chen, Y. (2018). A chlorinated low-bandgap small-molecule acceptor for organic solar cells with 14.1% efficiency and low energy loss. Sci. China Chem. *61*, 1307-1313.

16. Huang, C. *et al.* (2018). Highly efficient organic solar cells based on s,n-heteroacene non-fullerene acceptors. Chem. Mater. *30*, 5429-5434.

17. Gao, W. *et al.* (2018). Asymmetrical small molecule acceptor enabling nonfullerene polymer solar cell with fill factor approaching 79%. ACS Energy Lett. *3*, 1760-1768.

18. Fei, Z. *et al.* (2018). An alkylated indacenodithieno[3,2-b]thiophene-based nonfullerene acceptor with high crystallinity exhibiting single junction solar cell efficiencies greater than 13% with low voltage losses. Adv. Mater. *30*, 1705209.

19. Fan, Q. *et al.* (2018). Chlorine substituted 2d-conjugated polymer for high-performance polymer solar cells with 13.1% efficiency via toluene processing. Nano Energy *48*, 413-420.

20. Zhu, J. *et al.* (2018). Naphthodithiophene-based nonfullerene acceptor for high-performance organic photovoltaics: Effect of extended conjugation. Adv. Mater. *30*, 1704713.

21. An, Q. *et al.* (2018). Energy level modulation of non-fullerene acceptors enables efficient organic solar cells with small energy loss. J. Mater. Chem. A *6*, 2468-2475.

22. Xu, X., Yu, T., Bi, Z., Ma, W., Li, Y., and Peng, Q. (2018). Realizing over 13% efficiency in green-solvent-processed nonfullerene organic solar cells enabled by 1,3,4-thiadiazole-based wide-bandgap copolymers. Adv. Mater. *30*, 1703973.

23. Zhao, W., Li, S., Yao, H., Zhang, S., Zhang, Y., Yang, B., Hou, J. Molecular optimization enables over 13% efficiency in organic solar cells. *J. Am. Chem. Soc.* **139**, 7148-7151 (2017).

24. Zhao, F. *et al.* (2017). Single-junction binary-blend nonfullerene polymer solar cells with 12.1% efficiency. Adv. Mater. *29*, 1700144.

25. Xu, S., Zhou, Z., Liu, W., Zhang, Z., Liu, F., Yan, H., and Zhu, X. (2017). A twisted thieno[3,4-*b*]thiophene-based electron acceptor featuring a 14-π-electron indenoindene core for high-performance organic photovoltaics. Adv. Mater. *29*, 1704510.

26. Li, S., Ye, L., Zhao, W., Liu, X., Zhu, J., Ade, H., and Hou, J. (2017). Design of a new small-molecule electron acceptor enables efficient polymer solar cells with high fill factor. Adv. Mater. *29*, 1704051.

27. Li, S., Ye, L., Zhao, W., Zhang, S., Mukherjee, S., Ade, H., and Hou, J. (2016). Energy-level modulation of small-molecule electron acceptors to achieve over 12% efficiency in polymer solar cells. Adv. Mater. *28*, 9423-9429.

28. Yuan, J. *et al.* (2019). Single-junction organic solar cell with over 15% efficiency using fused-ring acceptor with electron-deficient core. Joule *3*, 1140-1151.

29. Zou, Y., Dong, Y., Sun, C., Wu, Y., Yang, H., Cui, C., and Li, Y. (2019). High-performance polymer solar cells with minimal energy loss enabled by a main-chain-twisted nonfullerene acceptor. Chem. Mater. *31*, 4222-4227.

30. Wang, T. *et al.* (2019). A wide-bandgap d–a copolymer donor based on a chlorine substituted acceptor unit for high performance polymer solar cells. J. Mater. Chem. A *7*, 14070-14078.

31. Wang, Q., Li, M., Zhang, X., Qin, Y., Wang, J., Zhang, J., Hou, J., Janssen, R. A. J., and Geng, Y. Carboxylate-substituted polythiophenes for efficient fullerene-free polymer solar cells: The effect of chlorination on their properties. Macromolecules DOI: 10.1021/acs.macromol.9b00793.

32. Liu, T. *et al.* A nonfullerene acceptor with 1000 nm absorption edge enables ternary organic solar cells with improved optical and morphological properties and efficiencies over 15%. Energy Environ. Sci. DOI: 10.1039/C9EE01030K.

33. Liu, T. *et al.* (2019). A high-performance non-fullerene acceptor compatible with polymers with different bandgaps for efficient organic solar cells. Sol. RRL *3*, 1800376.

34. Gao, H. H. *et al.* Achieving both enhanced voltage and current through fine-tuning molecular backbone and morphology control in organic solar cells. Adv. Energy Mater. DOI: 10.1002/aenm.201901024.

35. Cui, Y. *et al.* (2019). Over 16% efficiency organic photovoltaic cells enabled by a chlorinated acceptor with increased open-circuit voltages. Nat. Commun. *10*, 2515.

NMR Charts
Compound 2

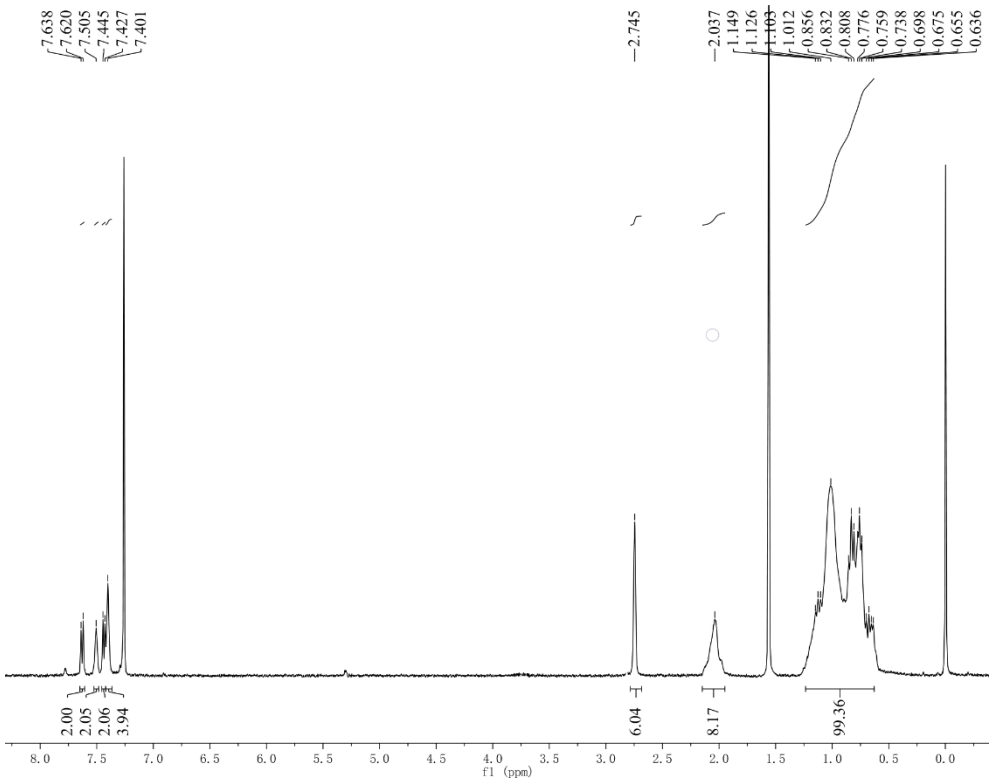

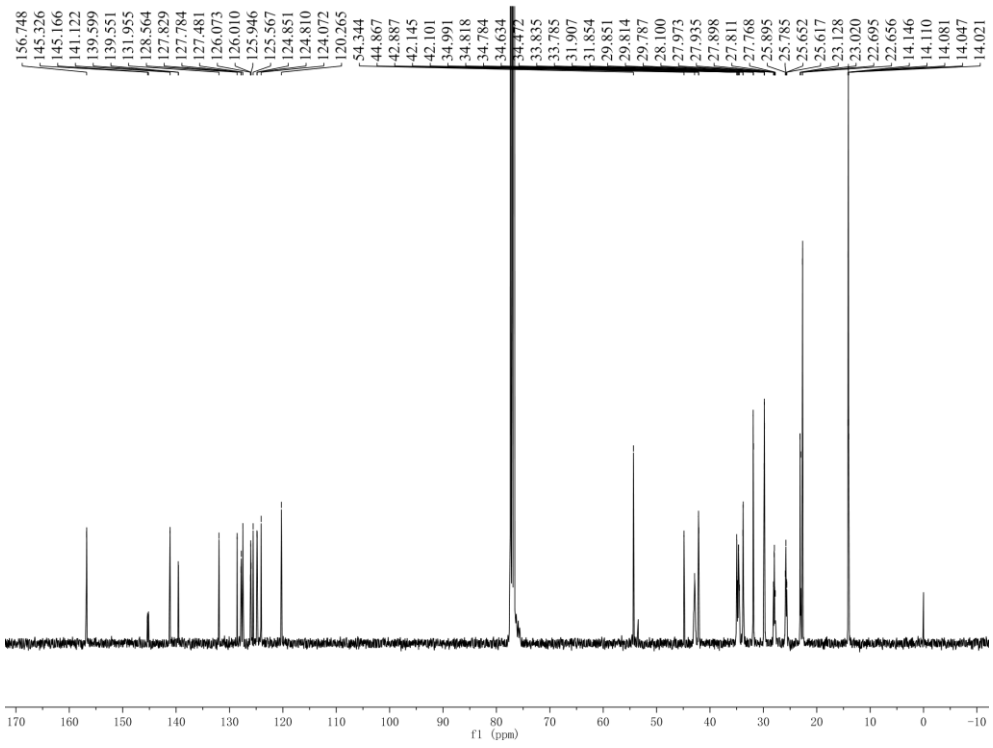

Compound IIDT-S

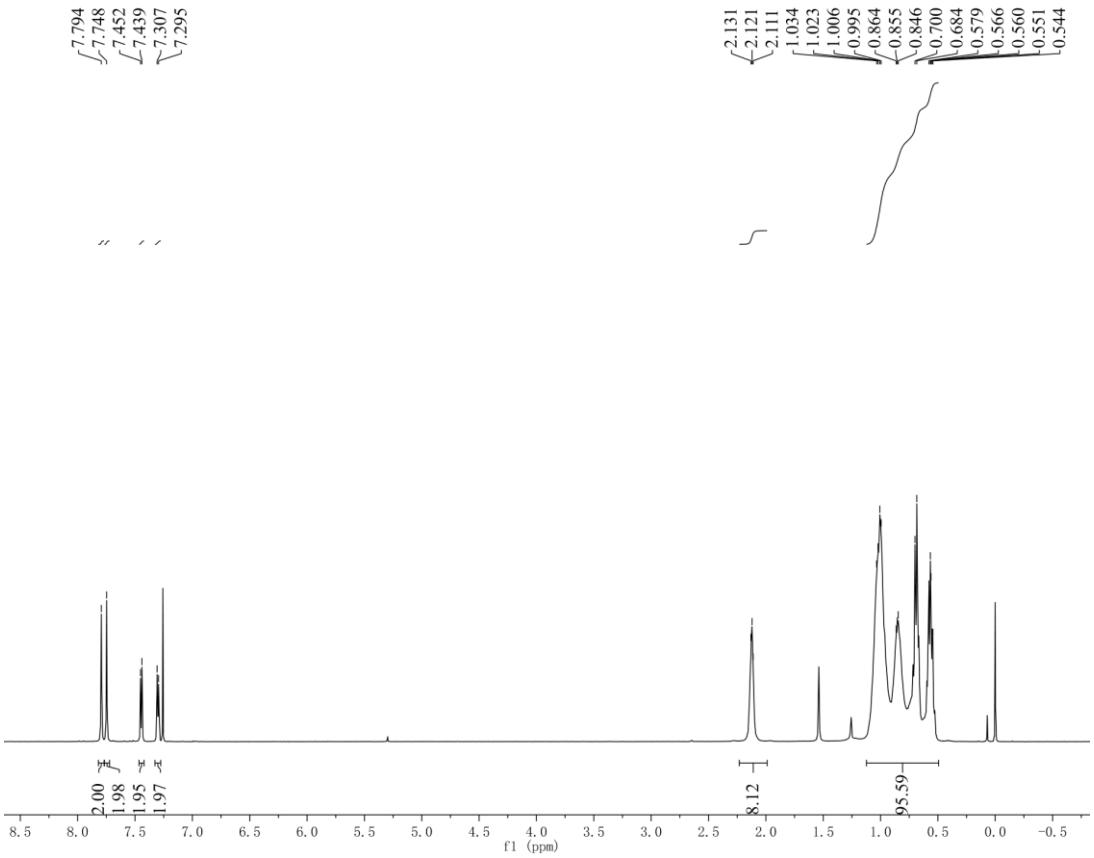

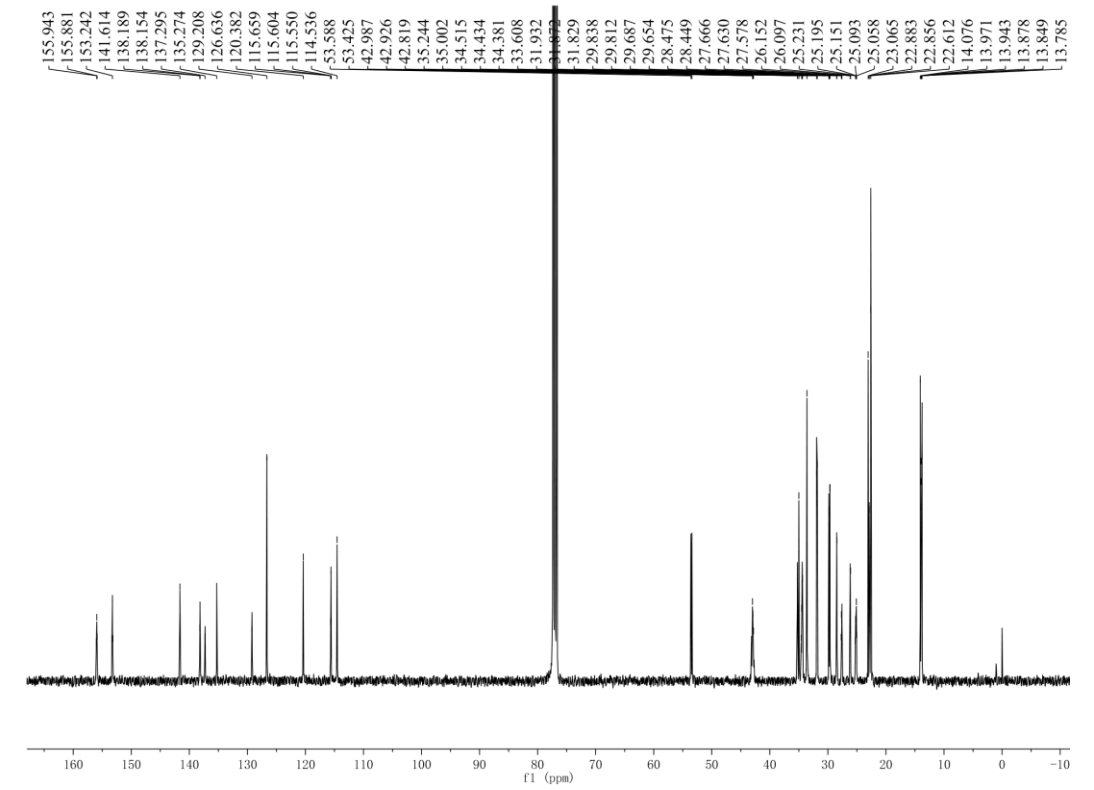

Compound IIDT-N

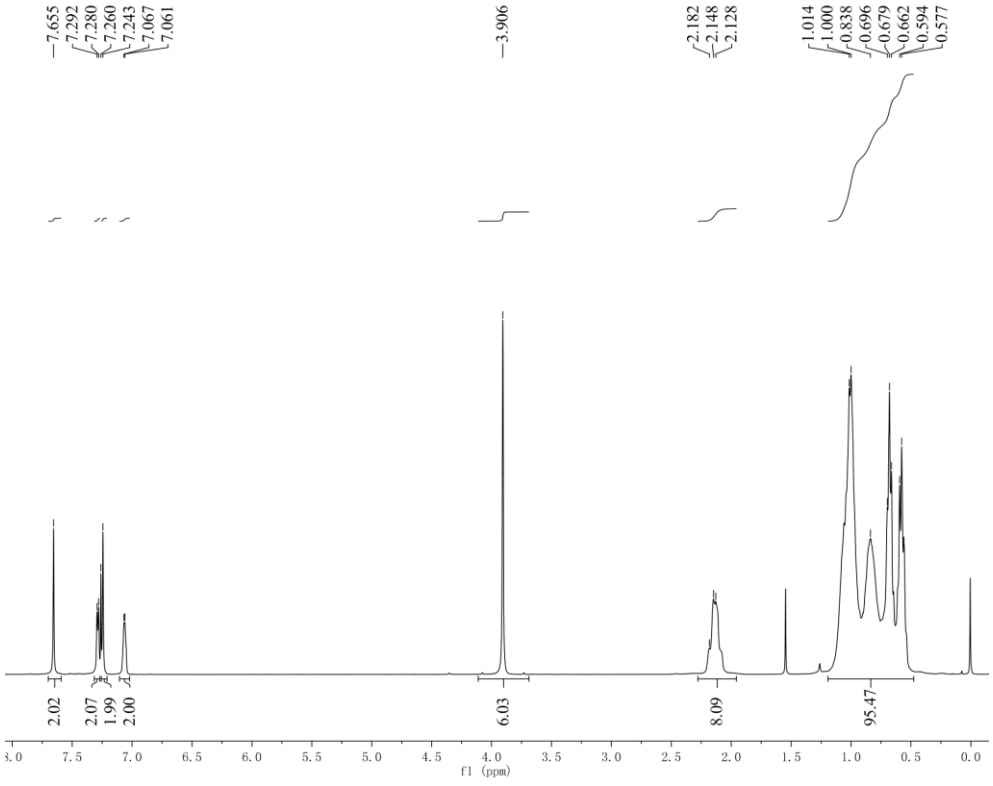

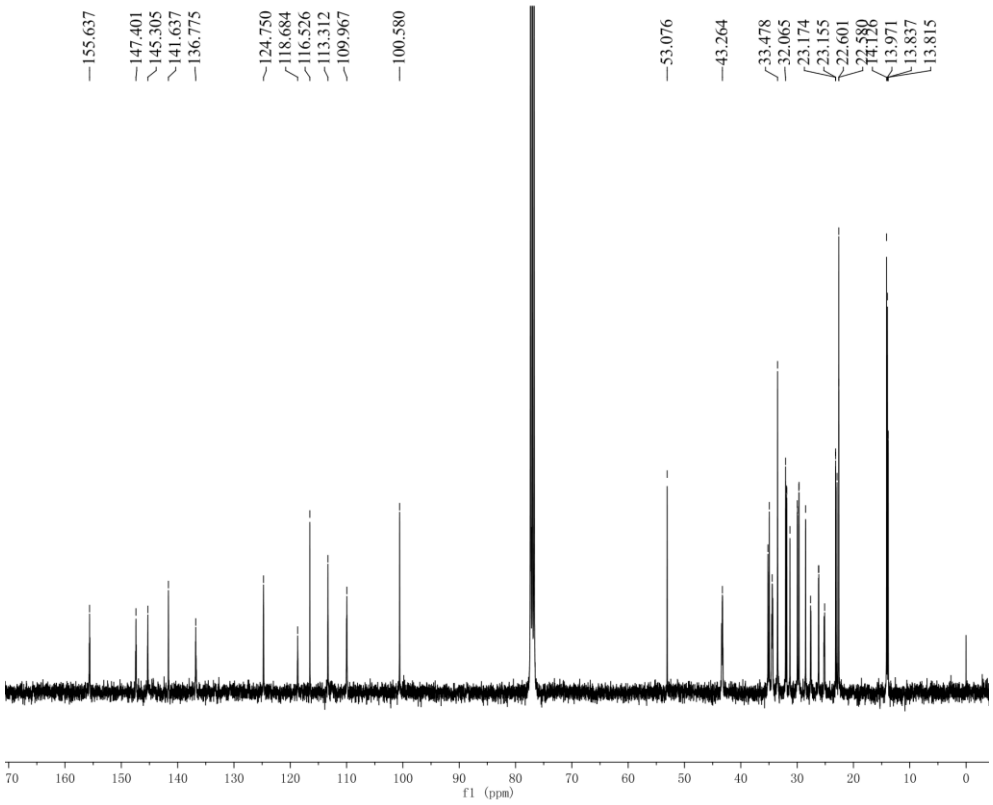

Compound 5-S

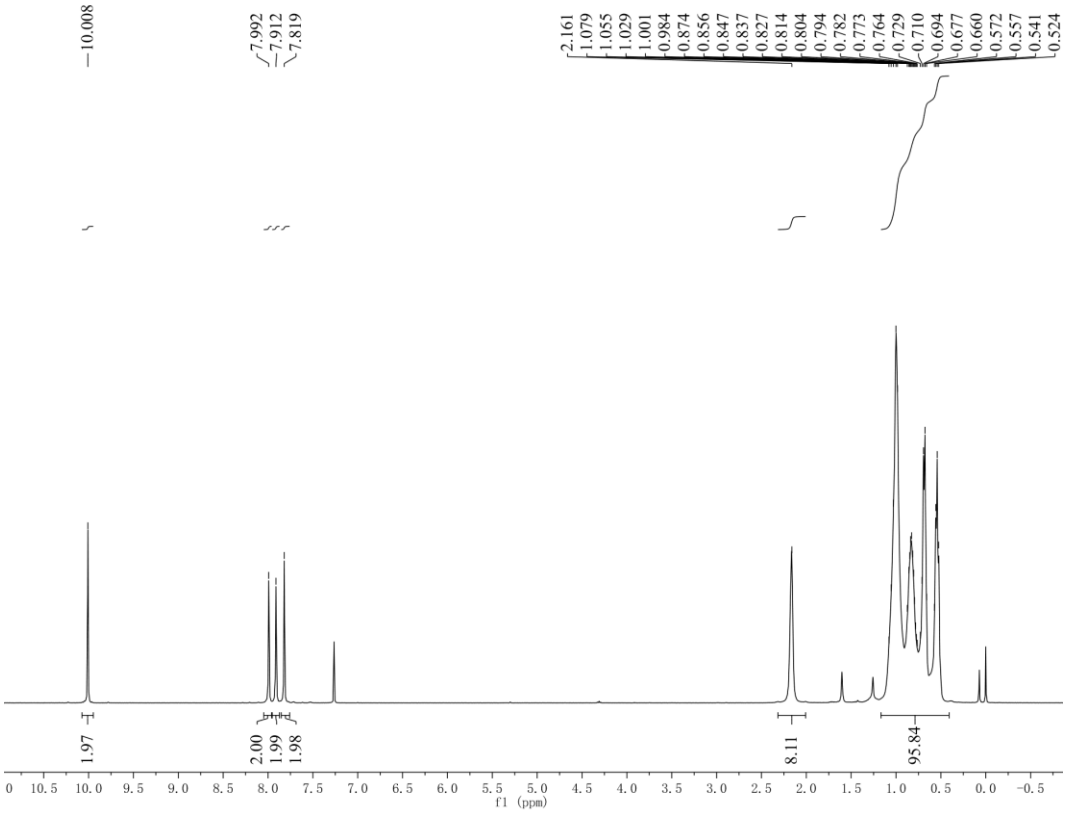
10.008
7.992
7.912
7.819
2.161
1.079
1.055
1.029
1.001
0.984
0.874
0.856
0.847
0.837
0.827
0.814
0.804
0.794
0.782
0.773
0.764
0.729
0.710
0.694
0.677
0.660
0.572
0.557
0.541
0.524
1.97
2.00
1.99
1.98
8.11
95.84
f1 (ppm)

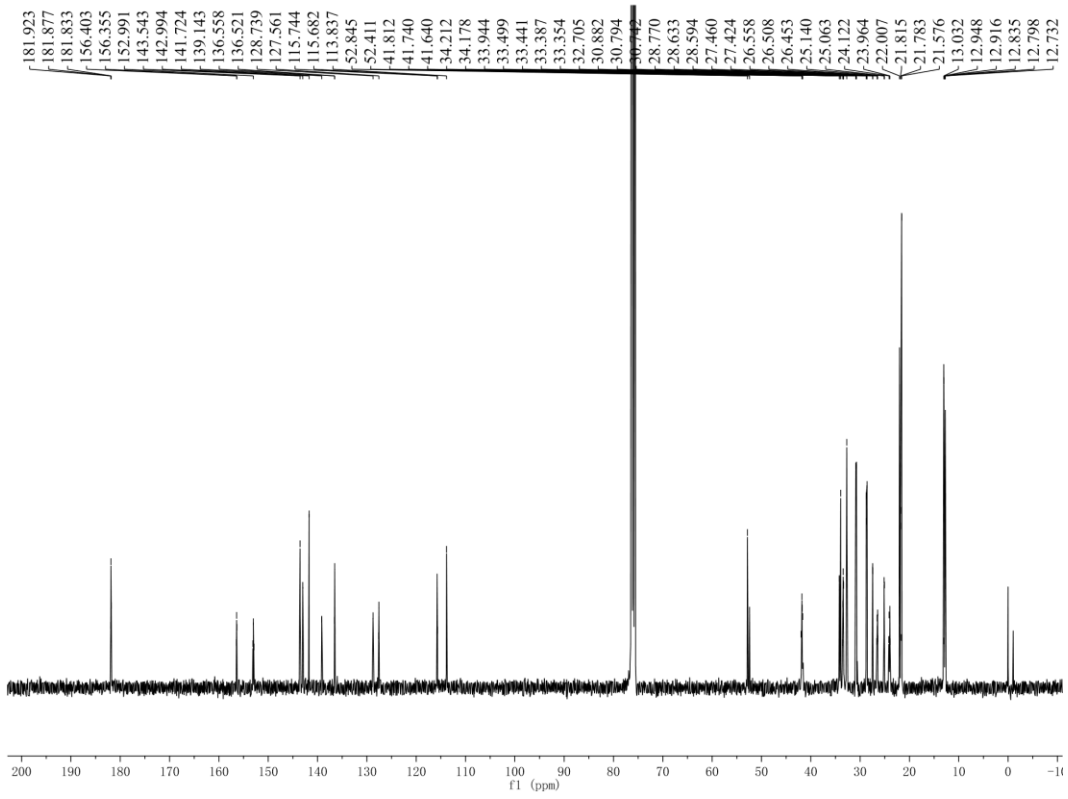
181.923
181.877
181.833
156.403
156.355
152.991
143.543
142.994
141.724
139.143
136.558
136.521
128.739
127.561
115.744
115.682
113.837
52.845
52.411
41.812
41.740
41.640
34.212
34.178
33.944
33.499
33.441
33.387
33.354
32.705
30.882
30.794
28.770
28.633
28.594
27.460
27.424
26.558
26.508
26.453
25.140
25.063
24.122
23.964
22.007
21.815
21.783
21.576
13.032
12.948
12.916
12.835
12.798
12.732
f1 (ppm)

Compound 5-N

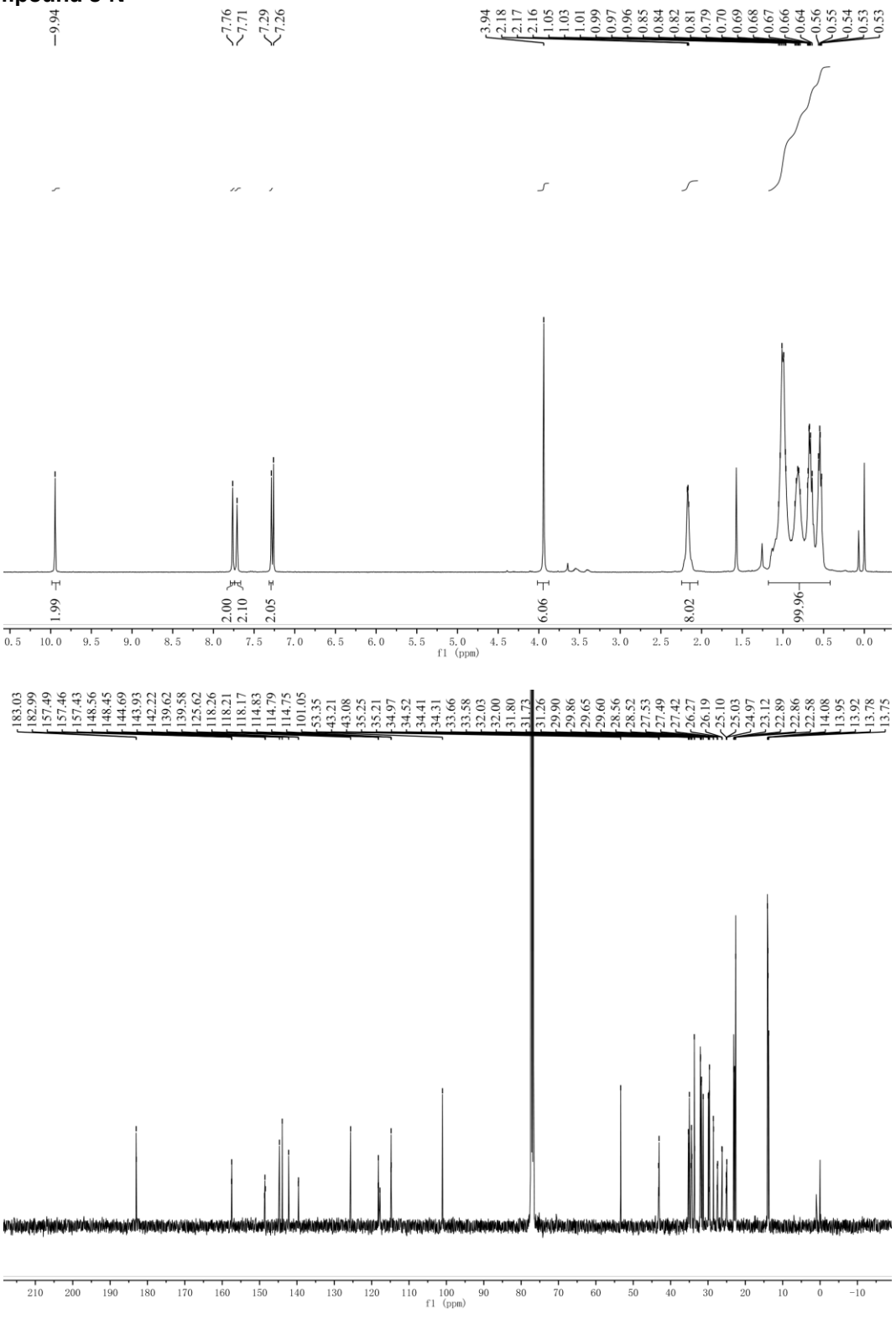
9.94
7.76
7.71
7.29
7.26
3.94
2.18
2.17
2.16
2.05
1.03
1.01
0.99
0.97
0.96
0.85
0.84
0.82
0.81
0.79
0.70
0.69
0.68
0.67
0.66
0.64
0.56
0.55
0.54
0.53
0.53
1.99
2.00
2.10
2.05
6.06
8.02
99.96
f1 (ppm)
183.03
182.99
157.49
157.46
157.43
148.56
148.45
144.69
143.93
142.22
139.62
139.58
125.62
118.26
118.21
118.17
114.83
114.79
114.75
101.05
53.35
43.21
43.08
35.25
35.21
34.97
34.52
34.41
34.31
33.66
33.58
32.03
32.00
31.80
31.73
31.26
29.90
29.86
29.65
29.60
28.56
28.52
27.53
27.49
27.42
26.27
26.19
25.10
25.03
24.97
23.12
22.89
22.86
22.58
14.08
13.95
13.92
13.78
13.75
f1 (ppm)

Compound ZITI-S

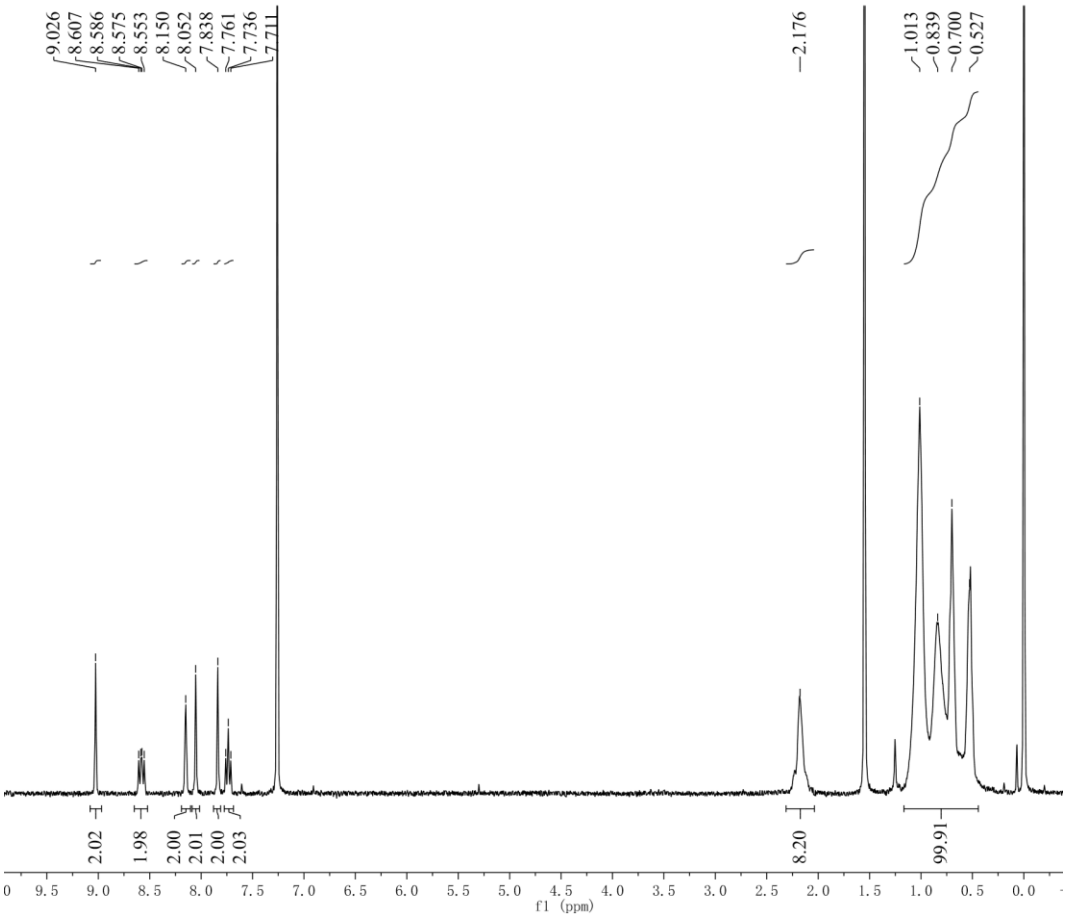

Compound ZITI-C

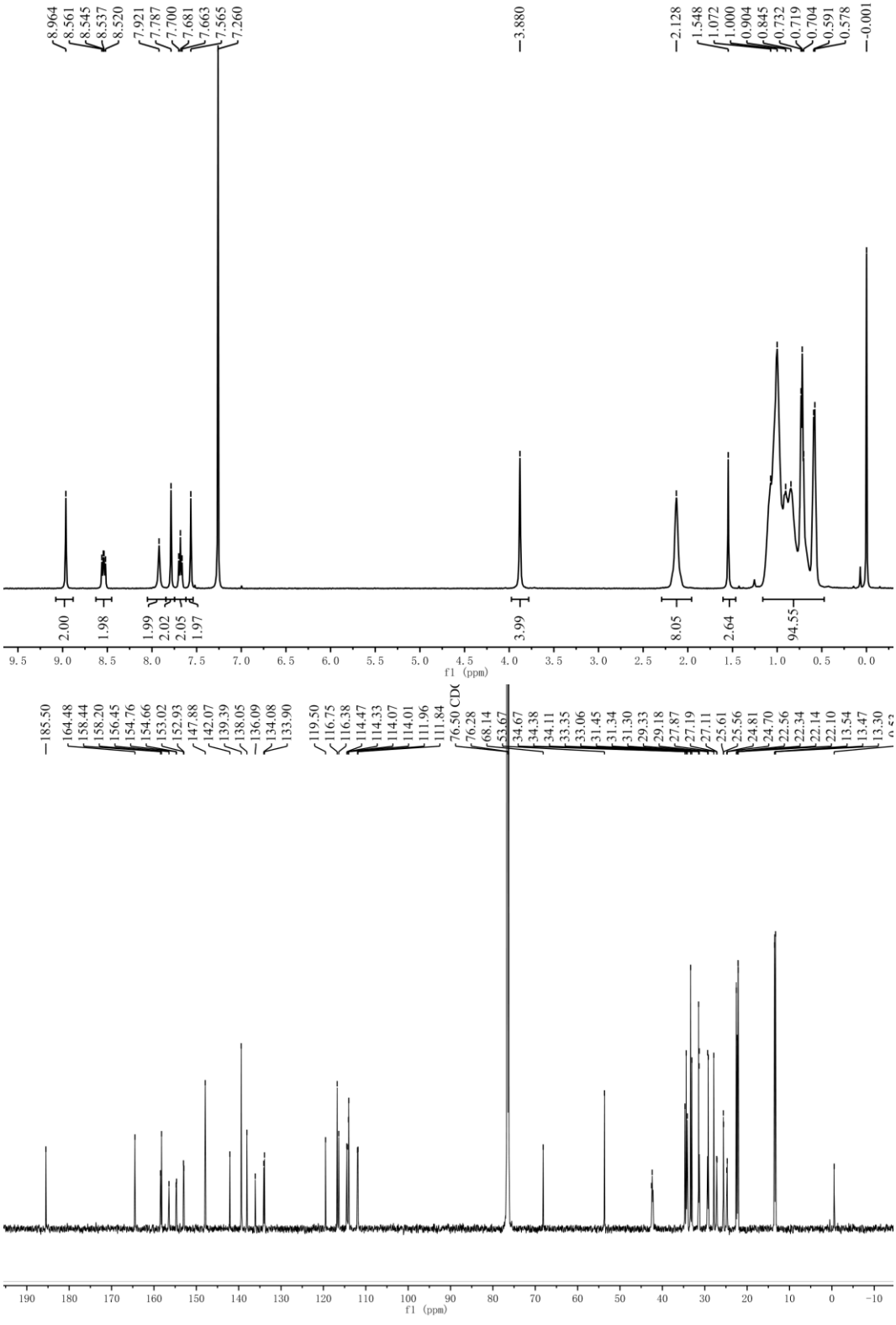

Compound ZITI-N